# System reliability analysis of soil nail wall using random finite element method

A. Johari [1] · A. Khosravi Hajivand [1] · S.M. Binesh [1]

## Abstract

Soil nail wall is a compound system which for safety margin determination, consideration of safety factors of its components and their correlations is required. In this paper, considering a real site using the random finite element method (RFEM), the reliability indices of global stability, lateral displacement stability, tensile strength, and pullout resistance stability as components of the soil nail wall system are obtained. In another section of the paper, using the sequential compounding method (SCM), the importance of the mentioned stability modes and their effects on system reliability and system probability of failure are represented. Results show that the most considerable interdependence is between the global and lateral displacement stabilities. Among the reliability indices of the components, the minimum one is attributed to the pullout resistance. Furthermore, the uppermost row of the nails has the most critical reliability index compared with the others. The locations of the slip surfaces and nail intersections varied from 0.05–0.90 of the nail length, which means that the uncertainty of the soil parameters has the most significant effect on the pullout resistance safety factor of the nails. The performance level of the soil nail wall decreases from below average to poor when the soil nail wall is considered to be a system with series components.

## Introduction

With increasing demands for appropriate infrastructures, designing excavations with vertical or near-vertical walls in urban areas is required more than ever. Among retaining wall systems, soil nailing is a suitable stabilizing approach for these types of excavations, particularly where top-to-bottom construction is advantageous.

Most of the methods for soil nail wall stability analysis are based on the limit equilibrium method (LEM) due to its simplicity and the reduced number of required parameters. In

typical design by LEM, three major requirements must be satisfied: external stability (global, sliding), internal stability (soil nail tensile strength and pullout), and facing stability (flexure and punching shear). In this group, well-known methods are presented by Stocker et al. (1979) (German method), Shen et al. (1981) (Davis method), Schlosser (1981) (French method), and Byrne et al. (1996) (FHWA manual). However, these methods are unable to predict the soil movement or simulate construction and installation processes. Furthermore, in all LEMs, assumptions regarding the characteristics of slip surfaces are essential in establishing the required equations. Thus, in practice, numerical methods such as finite element method (FEM) are usually implemented for the analysis of soil nail walls to overcome the limitations related to LEM and to consider the soil-structure interaction (Smith and Su 1997).

Numerous researches have focused on FEM techniques for soil nail wall analysis. Zhang et al. (1999) presented the extent and magnitude of deflection of a soil nail wall by a 3D FEM program. Shiu and Chang (2006) determined the maximum mobilized tensile forces in nails by FEM. Chang (2008) investigated the effective parameters on the slopes' safety factor (SF) by

✉ A. Johari
Johari@sutech.ac.ir

A. Khosravi Hajivand
A.Khosravi@sutech.ac.ir

S.M. Binesh
Binesh@sutech.ac.ir

1 Department of Civil and Environmental Engineering, Shiraz University of Technology, Shiraz, Iran

FEM. Sivakumar et al. (2007) analyzed a real vertical cut supported with retaining wall and soil nailing system, by 2D FEM program. Fan and Luo (2008) investigated the effect of nail inclinations on the stability of soil nail slope by non-linear FEM.

From another point of view, practical designs of soil nail walls have been done based on the Working or Allowable Stress Design (WSD or ASD, respectively) method in which soil parameters' heterogeneity is implemented by empirical safety factors. These methods cannot account for variability in both loading and resistance. To provide engineered designs with a consistent level of reliability, the Load and Resistance Factored Design (LRFD) method has been introduced by the American Concrete Institute (ACI) (ACI Committee and International Organization for Standardization, n.d.) wherein the uncertainties are quantified by probabilistic approaches. Some recent researches on soil nail wall design are developed based on the LRFD approach (e.g., (Lin and Liu 2017; Sivakumar Babu and Singh 2011; Lazarte 2011)).

Despite the success of the LRFD in importing uncertainties on geotechnical problem solutions, it cannot be utilized for direct reliability assessment of soil nail walls or in combination with the modes of stability. However, the stochastic analysis provides tools to overcome the above deficiencies by considering sources of uncertainties in obtaining reliability. For this reason, recently, stochastic analysis of the soil nail wall has been performed by several researchers. The soil parameter fluctuation for natural soil slope stability in conjunction with LEM has been utilized by Vanmarcke (1980), El-Ramly et al. (2002), Cho (2009), Li et al. (2015), and Javankhoshdel et al. (2017). Kitch (1994) performed stochastic analyses of two reinforced slopes by LEM. Low and Tang (1997) presented a reliability-based model for reinforced soft soil embankment stability.

In conventional soil nailing design procedures, six failure modes are considered, and each mode has its partial probability of failure and reliability index. Recently, a limited number of studies have been reported in the literature to consider the reliability of one or more non-correlated failure modes (e.g., (Sivakumar Babu and Singh 2011; Lin and Bathurst 2018; Bathurst et al. 2018; Babu and Singh 2009a; Lin et al. 2016)). While probabilistic soil nail wall stability analysis can be treated as a system reliability problem. The system reliability analysis presents a single reliability index for evaluation of the overall reliability, instead of the reliabilities of the components (Cho 2013; Zeng et al. 2015; Liu et al. 2018). The only research which is considered system reliability analysis has been accomplished by Zevgolis and Daffas (2018) where the LRFD approach, random variables, and system reliability are combined to consider the dependency of failure modes in soil nail walls.

The common feature of the mentioned stochastic studies was the consideration of spatial variability of soil properties by LEM in the soil nail wall. It should be noted that, without considering any of the underlying uncertainties in the whole

soil nail wall and also the interference and the efficacy of soil nail wall system components, designs are not bound to rigorous, reliable, and affordable results. To the authors' best knowledge, the stochastic analysis of the soil nail wall by RFEM with conjunction system reliability has not been investigated yet. The main objective of this research is to present a practical approach for system reliability analysis of soil nail wall via the random field theory. To achieve this aim, a real site of soil nail wall is considered. Then, the staged excavation analysis and calculation of the safety factors against the global stability, lateral displacement stability, tensile strength, and pullout resistance stability are carried out through a two-dimensional finite element-based program coded in MATLAB. The analysis is performed deterministically and then is extended to the probabilistic context to take into account the spatial variability of friction angle, cohesion, and unit weight. To obtain the reliability indices of the mentioned safety factors, the probability density functions (PDFs) of each of them are determined. In the next stage, the reliability indices of the mentioned safety factors are combined as a serial component of the system via their correlations to obtain the system reliability index of the soil nail wall.

## Methodology of analysis

### Finite element modeling of staged excavation

The FEM is a powerful tool, which can be utilized for soil nail wall modeling. The main advantage of FEM is providing information about deformations of the soil nail system. In this method, the SF and locations of critical failure planes are determined using the shear strength reduction method. In any soil nail wall modeling, staged excavation is needed.

If the project zone is excavated without supporting in one step, the wall during excavation can collapse. To prevent this situation, it is necessary to perform a step-by-step excavation and stabilization. On the other hand, this procedure creates an appropriate platform for nailing by the equipment.

For finite element modeling of the staged excavation, forces apply along the excavated surface; the remaining soil should experience the correct stress relief so that the new "free surface" is indeed stress-free (see surface "B" as shown in Fig. 1). Generally, the excavation forces $\{F_{BA}\}$ acting on a boundary depending on the stress state in the excavated material $\{\sigma_{A0}\}$ and on the self-weight of it can be calculated as follows (Smith et al. 2013).

$$\{F_{BA}\} = \int_{V_A} [B]^T \{\sigma_{A0}\} dV_A + \gamma \int_{V_A} [N]^T dV_A \qquad (1)$$

where $[B]$ is the strain-displacement matrix, $V_A$ the excavated volume, $\gamma$ the soil unit weight, and $[N]$ the shape functions of elements.

## Soil nailing modeling by finite element method

In plane strain FEM for modeling the soil nail wall, the nails are modeled by elements with rectangular shape and width equal to 1.0 m in the out-of-plane direction. For this purpose, plate or geogrid elements are used. In this way, the axial stiffness (EA) and the flexural stiffness (EI) are the most important nail material parameters. To model the grouted circular nails as rectangular shape elements, the equivalent axial stiffness is determined as follows:

$$\text{EA} = \frac{\left(E_n A_n + E_g A_g\right)\left(\pi D_{DH}^2\right)}{4AS_h} \qquad (2)$$

where $E_g$ is the grout elastic modulus, $E_n$ the nail elastic modulus, $D_{DH}$ the drill hole diameter, $S_h$ the nails horizontal spacing, $A = 0.25\pi D_{DH}^2$ the grouted soil nail cross-sectional area, $A_g = A\text{-}A_n$ the grout cover cross-sectional area, and $A_n = 0.25\pi d^2$ the nail cross-sectional area.

The bending stiffness of reinforcement permits a small extra shear force to be mobilized in the soil nail (Jewell and Pedley 1992; Pedley 1990). For these reasons, most soil nailing design methods (such as the USA, the UK (UK Department of Transport 1994), and Germany (Gassler 1996)) ignore the effects of shear force or bending stress mobilization in the nails. Thus, according to the code suggestion, in this research, the effect of bending stiffness is neglected.

## Soil nail wall stability analysis

Generally, for designing the soil nail walls, three major important stability analyses, namely, external stability (global and sliding), internal stability of soil nail (tensile strength and pullout), and facing stability (flexure and punching shear), have been considered (Bryne 1998).

External stability can be affected by the wall height, the width of the nailed area, the soil resistance, the nail resistance, and the interface resistance. Internal stability refers to

mechanisms of load transfer between the soil, the nail, and the grout. The tensile force in the nail gradually activates as excavation proceeds from top to bottom. By defining bond strength as the mobilized shear resistance along with the soil-grout interface, nail pullout stability is the stability along with the soil-grout interface because of sufficient bond strength or nail length. The pullout capacity of soil nails is a governing design parameter for the soil nailing technique. Therefore, the determination of accurate pullout capacity is necessary to ensure adequate internal stability of stabilized structures. High accuracy estimation of pullout resistance is difficult, as reflected in several attempts to fully understand it (e.g., (Tei et al. 1998; Davies et al. 1998; Li et al. 2008; Tan et al. 2008)). Flexure stability ought to be checked due to bending beyond the facing flexural capacity while punching shear, which should be assessed for both temporary and permanent facings, occurs around the nails' head.

## Stochastic analysis using random finite element method

The fluctuation in soil properties is the specific difference between geotechnical engineering and other areas of civil engineering. Physical and mechanical soil parameters change from one point in the field to another, which necessitates the expression of soil parameters as characterized by random fields (Vanmarcke 2010). In the theory of random fields, the soil parameters are uncertain quantities at any location of domain, which is characterized by probability distributions and the correlation between them. The spatial correlation of soil parameter is considered by auto-correlation function. Among such well-known functions, the Markov correlation function (Puła and Chwała 2015) is utilized because of its conservativeness and simplicity. However, other various forms of auto-correlation functions such as simpler Pearson, triangular, polynomial decaying, and also Gaussian auto-correlation functions can be employed in a random field generator (Griffiths and
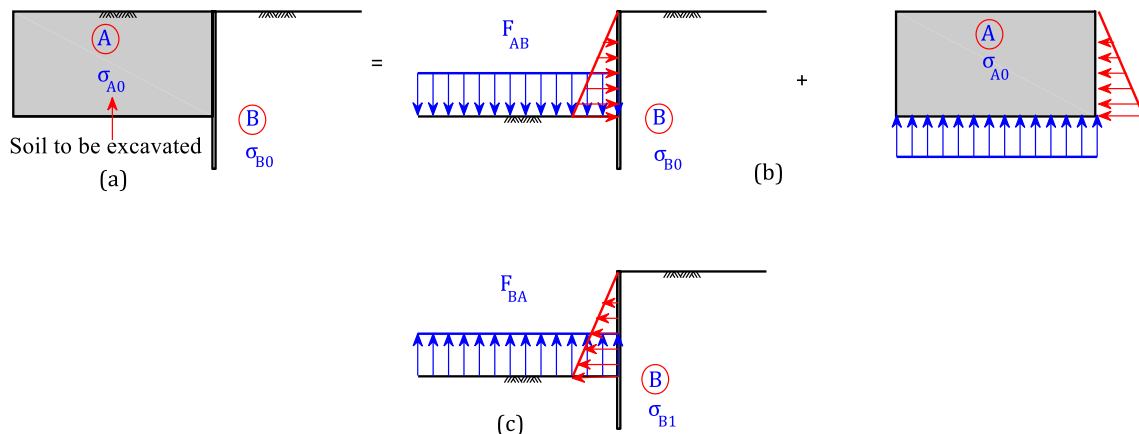


Fig. 1 The procedure of obtaining excavation forces (a): Initial stress state (b): Equilibrium of the bodies (A and B) (c): Excavation forces FBA

Fenton 2008; Fenton 1999). The Markov correlation function is:

$$\rho(x_1, x_2) = \exp\left(\frac{-|x_1 - x_2|}{l_x} - \frac{|y_1 - y_2|}{l_y}\right) \quad (3)$$

where $\rho(x_1, x_2)$ is a correlation matrix between sample points, $x_1$ and $x_2$ are spatial coordinates, and $l_x$ and $l_y$ correlation lengths in horizontal and vertical directions, respectively.

Among stochastic analysis methods for slope stability (Zeng et al. 2015; Johari and Javadi 2012; Johari and

**Fig. 2** Employing procedure for developing the computer program for system reliability analysis
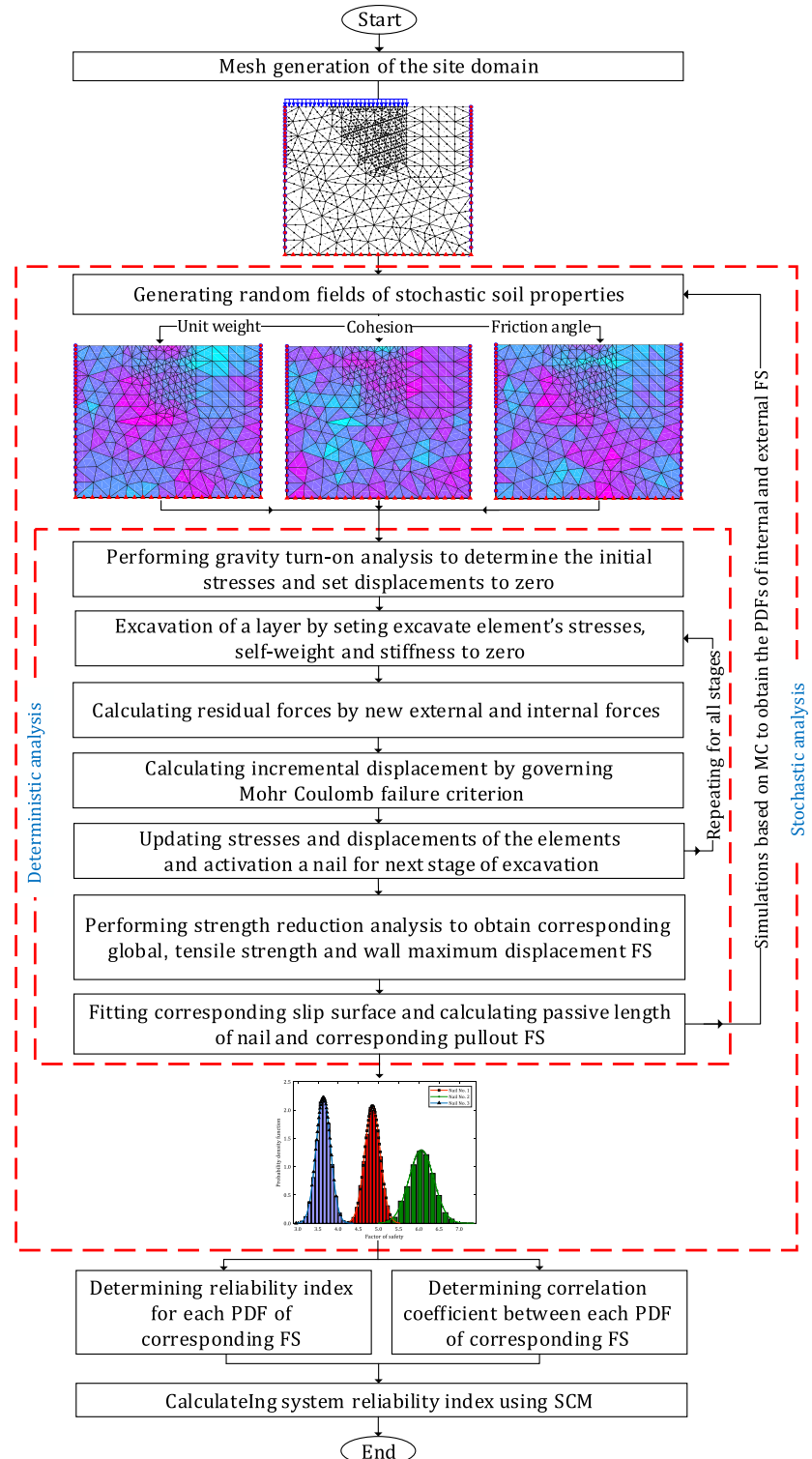
**Table 1** The adopted parameters for numerical simulations (Babu and Singh 2009b)

| Parameters | Values |
|---|---|
| Cohesion, $c$ (kPa) | 4.0 |
| Internal friction angle, $\phi$ (Deg.) | 31.5 |
| Unit weight, $\gamma$ (kN/m$^3$) | 17.0 |
| Elasticity modulus, $E_s$ (MPa) | 20.0 |
| Poisson's ratio of soil, $_s$ | 0.3 |
| Grouted nails and facing | |
| Material model | Elastic |
| Yield strength of reinforcement, $f_y$ (MPa) | 415.0 |
| Elasticity modulus of reinforcement, $E_n$ (GPa) | 200.0 |
| Elasticity modulus of grout (concrete), $E_g$ (GPa) | 22.0 |
| Diameter of reinforcement, $d$ (mm) | 20.0 |
| Drill hole diameter, $D_{DH}$ (mm) | 100.0 |
| Length of the nail, $L$ (m) | 7.0 |
| Declination with respect to horizontal, $i$ (Deg.) | 15.0 |
| Spacing $S_h \times S_v$ (m $\times$ m) | 1.0 $\times$ 1.0 |
| Facing thickness, $t$ (mm) | 200.0 |



Fig. 4 Deformed mesh after excavation

Mousavi 2018; Da Costa and Sagaseta 2010; Li et al. 2017; Johari and Gholampour 2018; Allahverdizadeh et al. 2015), RFEM using advantages of the FEM, by employing random field theory, offers a powerful tool to incorporate fluctuation of soil properties into reliability analysis of geotechnical problems such as slope stability (Johari and Gholampour 2018; Johari and Heydari 2018) and soil nail wall.
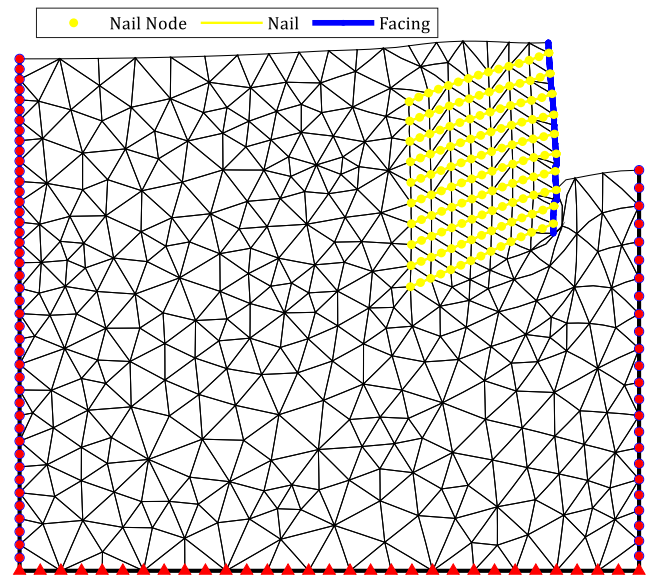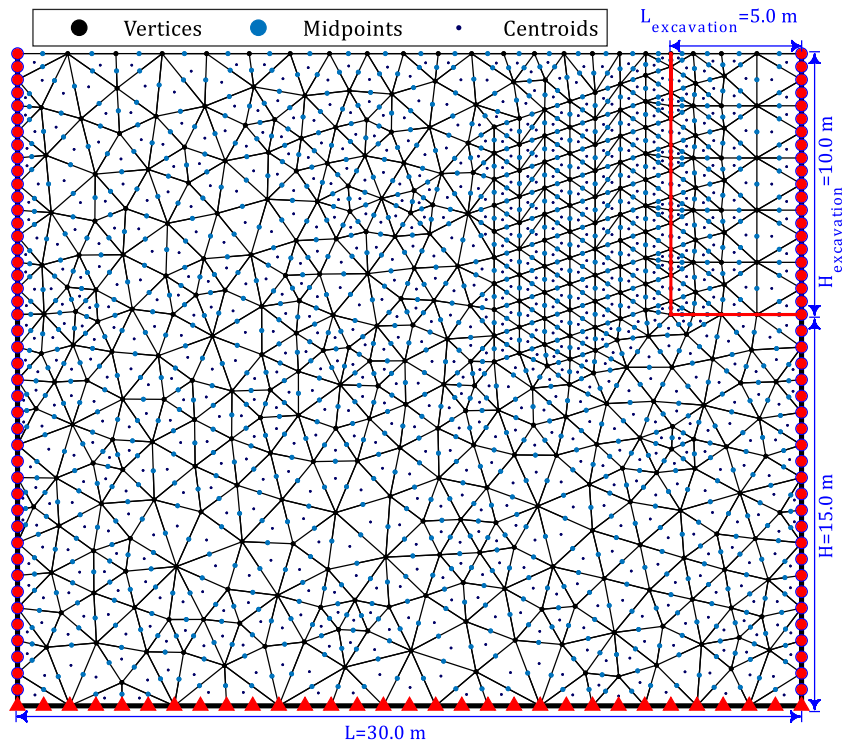
## System reliability analysis

Physical systems that are composed of multiple components can be classified as parallel, series, or combined systems (Li et al. 2009). In a parallel system, all the components must fail to cause the system to fail completely. In a series system, the failure of one component should be able to eliminate the system completely. Furthermore, many stochastic problems are complex to an extent where the exact direct calculation of the reliability index is completely impossible. Such complex

Fig. 3 Geometry and initial mesh of excavation

systems can be analyzed by calculating the reliabilities for the individual parallel and series components and then combining them in the appropriate manner (Zhang et al. 2011; Zhao et al. 2016).

## Sequential compounding method

Generally, in combining the components of a system, a direct numerical integration system approach is impractical in many cases because, as the number of component events increases, the significant numerical errors are accumulated, and computational cost is increased rapidly. The sequential compounding method (SCM) is one of the rigorous methods that are proposed for combining the components of a system (Kang and Song 2010). This method compounds two components coupled with a logical operation sequentially until the system event of interest is simplified into a single compound event. Since SCM deals with the logical operation of only two components each time, the compounding process would not be encumbered by the complexity of the logical description of a given general system (Kang and Song 2010).

Consider compounding two components $E_1$ and $E_2$ coupled by union into a single equivalent event $E_{1\ or\ 2}$. For example, this compounding can appear in a series system or a link-set system, and can be compounded as follows:

$$P(E_1 \cup E_2 \cup ... \cup E_{10}) = P(E_{1or2} \cup E_3 \cup ... \cup E_{10})$$
$$P((E_1 \cup E_2 \cup E_3) \cap (E_4 \cup E_5 \cup E_6)) = P((E_{1or2} \cup E_3) \cap (E_4 \cup E_5 \cup E_6)) \quad (4)$$

First, using De Morgan's rule and the symmetry of the standard normal distribution, the reliability index of the compound event $E_{1\ or\ 2}$ is obtained by:
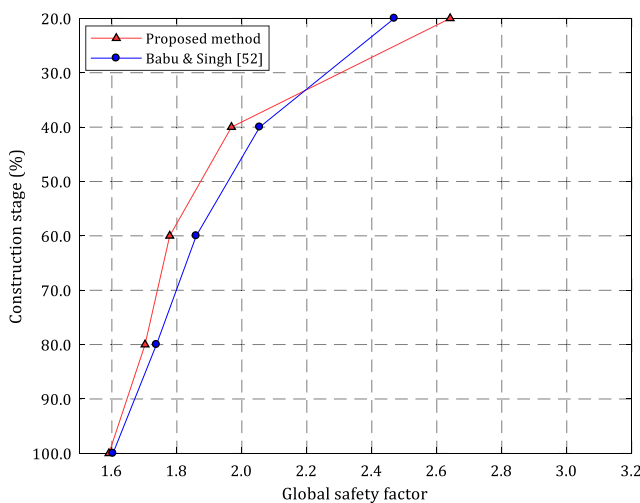
$$\beta_{1or2} = -\Phi^{-1}[P(E_1 \cup E_2)] = -\Phi^{-1}\left[1 - P\left(\overline{E}_1 \cap \overline{E}_2\right)\right]$$
$$= \Phi^{-1}\left[P\left(\overline{E}_1 \cap \overline{E}_2\right)\right]$$
$$= \Phi^{-1}\left[\Phi(\beta_1)\Phi(\beta_2) + \int_0^{\rho_{1,2}} \varphi_2\left(\beta_1, \beta_2, \rho\right)d\rho\right] \quad (5)$$

where $\beta_1$ and $\beta_2$ are the reliability indexes of $E_1$ and $E_2$, respectively, and $\rho_{12}$ is the correlation coefficient between the standard normal random variables $Z_1$ and $Z_2$, which respectively represents $E_1$ and $E_2$. Next, the aim is to find the equivalent correlation coefficient $\rho_{(1\ or\ 2),k}$ that would provide the same estimate on the probability of the following event:

$$\Omega_u = [(Z_1 \le -\beta_1) \cup (Z_2 \le -\beta_2)] \cap (Z_k \le -\beta_k) \quad (6)$$

After compounding, i.e.:

$$\int_{\Omega_u} \varphi_3\left(z_1, z_2, z_3; \rho_{1,2}, \rho_{1,k}, \rho_{2,k}\right)dz = \Phi_2\left(-\beta_{1or2}, -\beta_k; \rho_{(1or2),k}\right) \quad (7)$$

where $\Omega$ denotes the domain of a system event defined in the space of $n$ standard normal random variables.

Using the decomposition and approximation used in conditional probabilities, Eq. (7) is approximated as

$$1 - \Phi_2\left(\beta_{1|k}, \beta_{2|k}; \rho_{1,2|k}\right) = \Phi\left(-\beta_{(1or2)|k}\right) \quad (8)$$

where $\Phi_2(.)$ and $\Phi(.)$ respectively denote the joint cumulative distribution function (CDF) of the bivariate standard normal distributions and the cumulative distribution function of the standard normal distribution.

$$\beta_{(1or2)|k} = \left(\beta_{1or2} - \rho_{(1or2),k}A\right) / \sqrt{1 - \rho^2_{(1or2),k}B} \quad (9)$$

where $A = \varphi(-\beta_k)/\Phi(-\beta_k)$ and $B = A(-\beta_k + A)$ in which $\varphi(.)$ denotes the PDF of the standard normal distribution.
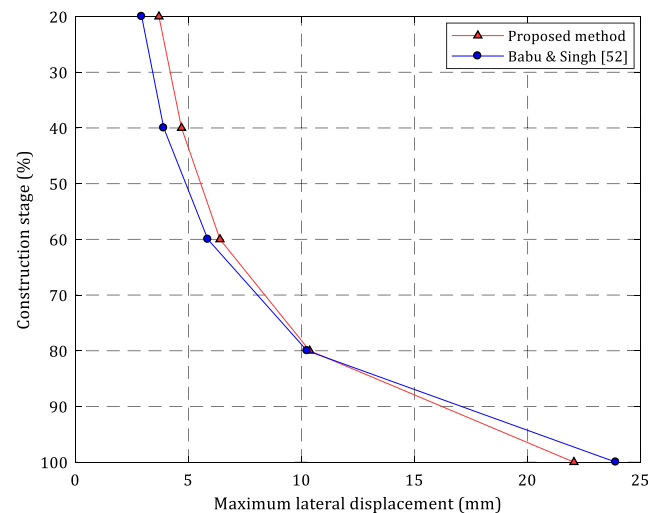


Fig. 5 Comparison of global safety factors of two models in stages of construction



Fig. 6 Comparison of maximum lateral displacements of two models in stages of construction

**Table 2** Comparison of the results of the two methods

| Methods | Safety factor | Maximum lateral displacement (mm) |
|---|---|---|
| Singh and Babu (2009b) | 1.603 | 23.90 |
| Proposed method | 1.591 | 22.05 |

The bi-variate CDF in Eq. (8) can be computed by performing the single-fold numerical integration as follows:

$$\Phi_2\left(\beta_{1|k}, \beta_{2|k}; \rho_{1,2|k}\right) = \Phi\left(\beta_{1|k}\right)\Phi\left(\beta_{2|k}\right) + \int_0^{\rho_{1,2|k}} \varphi_2\left(\beta_{1|k}, \beta_{2|k}; \rho\right)d\rho \qquad (10)$$

where at each compounding, Eqs. (8) and (9) are solved numerically for $\rho_{(1 \text{ or } 2),k}$ $k = 3, \ldots n$ where $n$ is the current total number of components in the system during a sequential compounding process with the constraint $-1 \le \rho_{(1 \text{ or } 2),k} \le 1$.

## The employed procedure of system reliability analysis of soil nail wall

In previous sections, the selected methodology of stochastic analysis for the soil nail wall was described. In this section, the practical implementation of the mentioned methodology is expressed. For this purpose, the procedure is schematically shown in Fig. 2. Based on this flowchart, the arranged procedure for system reliability analysis consists of three parts as follows:

(I)  Developing a computer program for deterministic analysis, including:

– Mesh generation of the site domain and gravity turn-on analysis
– Staged excavation analysis by governing the Mohr-Coulomb (MC) failure criterion
– Strength reduction analysis to obtain safety factors

(II)  Extend computer program for stochastic analysis by random field theory and Monte Carlo simulation (MCS)

(III)  Determination of system reliability index by combining reliability indices of components using SCM

## Computer programs and verification

In this study, a deterministic finite element-based program was coded in MATLAB to simulate the staged excavation and calculation of safety factors for the vertical soil nail wall. To assess the uncertainties of soil properties, the computer program was extended to combine random fields with the finite element.

The plane strain condition with two translation degrees of freedom along x- and y-axes is available in the coded program. In the plane strain model, the displacements and strains in the z-direction are assumed to be zero. However, normal stresses in the z-direction are considered. The two-dimensional calculations with 6-noded triangular elements were done in order to get fairly accurate results with regard to the capacity of the computational machine, and also
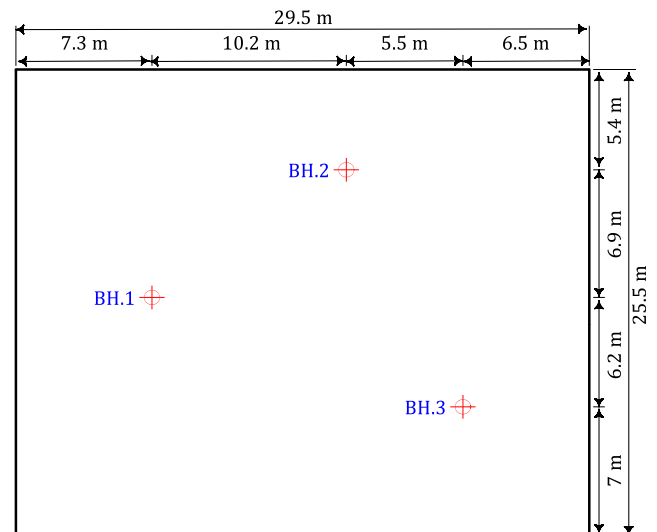


**Fig. 7** The situation of the site before excavation



**Fig. 8** The boreholes arrangement in the site plan

**Table 3** Soil properties from BH.1

| Depth | Unit weight (gr/cm$^3$) | Friction angle (Deg.) | Cohesion (kN/m$^2$) | Gravel content (%) | Sand content (%) | Clay content (%) | Fine-grained content (%) |
|---|---|---|---|---|---|---|---|
| 2 | 1.87 | 28.00 | 24.00 | 44.30 | 2.30 | 0.00 | 53.40 |
| 4 | 1.77 | | | 0.00 | 22.50 | 22.00 | 77.50 |
| 6 | 1.79 | 25.00 | 30.00 | 0.00 | 24.60 | 21.00 | 75.40 |
| 8 | 1.76 | | | 0.00 | 18.13 | 20.00 | 81.87 |
| 10 | 1.80 | 24.00 | 28.50 | 0.00 | 23.94 | 19.00 | 76.06 |
| 12 | 1.75 | | | 0.00 | 25.41 | 19.50 | 74.59 |
| 14 | 1.83 | 25.50 | 32.00 | 33.03 | 47.37 | 0.00 | 19.60 |
| 16 | 1.85 | | | 33.96 | 45.98 | 0.00 | 20.06 |

computational time. The 6-node triangle element is a fairly accurate element that gives good results in standard deformation analyses, which provides a second-order interpolation for displacements, and the numerical integration involves three Gauss points. The type of element for structural elements is taken to be compatible with the soil element type.

The favorable geometric properties of the Delaunay triangulation make it suitable for use in this study. For a set of points in 2D, a Delaunay triangulation of these points ensures the circumcircle associated with each triangle contains no other point in its interior (George 1991). The coded program involves automatic mesh generation, which can produce an unstructured mesh. Unstructured meshing allows efficient element arrangement and refinement of the element in the vicinity of the important points such as those along with the nails, which is crucial for the accurate prediction of the results. The mesh generation is based on a robust triangulation procedure. A global refinement to increase the number of elements globally and a line refinement to increase the element numbers along the nails are available to obtain better results. While the number of mesh elements considerably affects the results, sensitivity study on mesh elements for each analysis should be investigated. The sensitivity analysis was conducted until there was no meaningful difference in two particular

succession results. Thus, the most appropriate mesh density was chosen.

The program was developed for the 2D, plane strain condition using six-node triangular elements of elastic perfect-plastic soil behavior with the Mohr-Coulomb failure criterion. The computer program has the capability of changing the geometry, nail inclination, finding maximum accumulated deviatoric plastic strain points, potential slip surface, and soil nail interface modeling.

To verify the coded program, a soil nail wall which has been modeled by Singh and Babu (2009b) is considered. The presented modeling is covering a 10.0-m excavation by 10 nail activation in 5 stages. The model parameters are listed in Table 1. For verification, the 30.0 m by 25.0 m domain consisted of 265 six-noded triangular elements, as shown in Fig. 3. However, coarse mesh density globally and fine mesh density in the vicinity of the soil nail wall was used by Singh and Babu (2009b); in this part of research, to ensure reasonably accurate results, a globally medium mesh was chosen, and for greater accuracy, the meshes between the layers of reinforcing bars were further refined. The boundary conditions of the domain were specified by horizontally restraining the left and the right sides and fully restraining the bottom side. Two-dimensional 3-node bar elements are chosen to

**Table 4** Soil properties from BH.2

| Depth | Unit weight (gr/cm$^3$) | Friction angle (Deg.) | Cohesion (kN/m$^2$) | Gravel content (%) | Sand content (%) | Clay content (%) | Fine-grained content (%) |
|---|---|---|---|---|---|---|---|
| 2 | 2.02 | | | 38.70 | 18.70 | 0.00 | 42.60 |
| 4 | 1.75 | 25.00 | 27.00 | 2.00 | 28.00 | 19.00 | 70.00 |
| 6 | 1.72 | | | 0.00 | 22.55 | 19.00 | 77.45 |
| 8 | 1.69 | 26.00 | 28.50 | 0.00 | 21.09 | 20.00 | 78.91 |
| 10 | 1.62 | | | 0.00 | 17.43 | 20.00 | 82.57 |
| 12 | 1.79 | 23.00 | 32.00 | 0.00 | 23.58 | 20.00 | 76.42 |
| 14 | 1.81 | | | 0.00 | 20.28 | 20.00 | 79.72 |
| 16 | 1.89 | | | 55.49 | 32.92 | 0.00 | 11.59 |

**Table 5** Soil properties from BH.3

| Depth | Unit weight (gr/cm$^3$) | Friction angle (Deg.) | Cohesion (kN/m$^2$) | Gravel content (%) | Sand content (%) | Clay content (%) | Fine-grained content (%) |
|---|---|---|---|---|---|---|---|
| 2 | 1.89 | 33.00 | 23.00 | 40.50 | 26.70 | 0.00 | 32.80 |
| 4 | 1.82 | | | 11.00 | 11.20 | 17.00 | 77.80 |
| 6 | 1.76 | 25.50 | 27.00 | 0.00 | 17.48 | 20.00 | 82.52 |
| 8 | 1.79 | | | 0.00 | 15.35 | 21.00 | 84.65 |
| 10 | 1.77 | 26.00 | 29.00 | 0.00 | 28.97 | 19.00 | 71.03 |
| 12 | 1.79 | | | 0.00 | 21.88 | 20.00 | 78.12 |
| 14 | 1.69 | | | 0.00 | 19.21 | 22.00 | 80.79 |
| 16 | 1.94 | 25.00 | 27.00 | 67.84 | 10.59 | 0.00 | 21.57 |

simulate the nails. The nails are modeled as elastic material and the bending stiffness is neglected.

After all excavation stages, the deformed mesh, uniformly magnified to emphasize the deformations, is shown in Fig. 4. A comparison of safety factor and maximum lateral deformation with the stages of construction is shown in Figs. 5 and 6, respectively. Furthermore, the results of the analysis are given in Table 2.

In general, in each excavation analysis, the excavation forces acting on a boundary depend on the stress state in the excavated material and on the self-weight of that material. When the situation is two- or three-dimensional, in the corners of excavations, a rather complex stress concentration exists. This means that the finite element results will be mesh-dependent, as it is concluded by Smith and Ho (1992). However, the denser or higher-order mesh may consequence in more accurate analysis. It is important to note that increasing the mesh density and order results in a drastic increase in the overall calculation time. Thus, appropriate mesh density and order shall be used depending upon the degree of accuracy required and the capacity of the computing machine. Although the analyses were carried out by two different mesh densities and element types, the results are reasonably close.

### Geotechnical characteristics of the site

To demonstrate the applicability of the provided procedure in the system reliability of the soil nail wall, a real site is presented in this section. For this purpose, a real site with 8.0 m depth

**Table 6** Geotechnical site soil parameters

| Parameters | Values |
|---|---|
| Cohesion, $c$ (kN/m$^2$) | 28.0 |
| Friction angle, $\phi$ (Deg.) | 26.0 |
| Unit weight, $\gamma$ (kN/m$^3$) | 18.0 |
| Modulus of elasticity, $E$ (kN/m$^2$) | 30,000.0 |
| Poisson's ratio, $\upsilon$ | 0.3 |

of excavation in Shiraz city in Iran was considered. The similar excavation geometry with respect to out of plane dimension would make the site suitable for plane strain modeling. Figure 7 shows the situation of the site and adjacent structures before excavation.

In order to specify the soil profile of the site, three boreholes were drilled to the depth of 16.0 m from the natural ground surface. The dimension of the site and the borehole arrangement are shown in Fig. 8. For each borehole, the laboratory tests (i.e., grain size analysis, Atterberg limits tests, and so on) were performed. The borehole database is given in Tables 3, 4, and 5. The mean geotechnical site soil parameters are given in Table 6.

### Soil nailing modeling

The verified coded program was utilized for analyzing a real soil nail wall in this section. The general conditions of the real vertical cut, such as its geometry of the model, surcharge, and
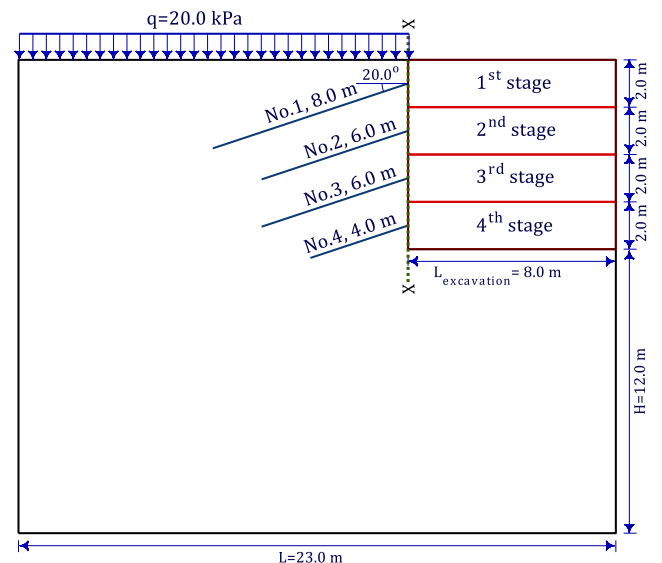


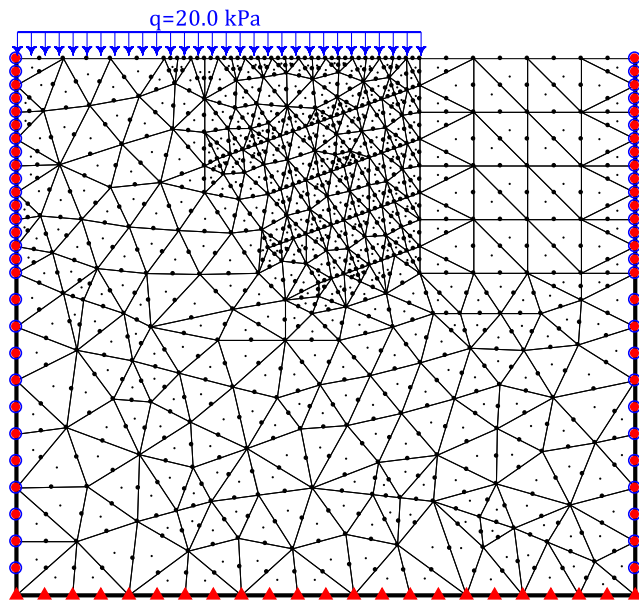**Fig. 9** The studied soil nail wall and excavation characteristics

**Fig. 10** The initial mesh of soil nail wall and excavation



**Fig. 11** Nail configuration for studied soil nail wall

nail characteristics, are shown in Fig. 9. Furthermore, the related finite element discretization with boundary conditions is illustrated in Fig. 10. For this purpose, at the bottom boundary of the finite element mesh, the two horizontal and vertical degrees of freedom are fixed. At the lateral boundaries, only the horizontal degree of freedom, corresponding to the axis, is fixed. The distances of the bottom and lateral boundaries from the facing varied from analysis to analysis in order to ensure that the boundaries did not interfere with the development of the collapse mechanism while maintaining adequate mesh density close to the nails. Also, for modeling the surcharge due to adjacent structures, a uniform load was applied to those nodes representing the surface. It should be mentioned that the bending stiffness of the nails was ignored. For determining the more accurate result, the shotcrete can be implemented in modeling; however, to avoid the computational cost in iterative stochastic analysis, in this research, it was neglected. The selected nail design parameters are presented in Table 7 followed by Fig. 11 which illustrates a section of the nail configuration. However, the use of advanced soil models provides more realistic results of the simulated structures. It becomes desirable to assess the implications of the use of advanced soil models over conventional Mohr-Coulomb model

in case of the capacity of the computers, computational time, and accuracy of geotechnical investigations in concern.

The uniformly magnified deformed meshes after each stage of excavation are shown in Figs. 12, 13, 14, 15, and 16. The red arrows in these figures stand for the magnified resultant of two horizontal and vertical displacement vectors acting in respective nodes. After each stage of excavation, the SF was calculated using the strength reduction method. Lateral displacements for different depths and stages of the excavation are illustrated in Fig. 17. This figure shows that as expected, the lateral displacement of different depths of the excavation increases progressively. In the last stage of excavation, the maximum lateral displacements occurred at about 1.0 m from the bottom of the excavation. The maximum lateral displacement was found to be equal to 18.87 mm. Also, the maximum lateral displacement at the top of the wall was 11.16 mm, which is less than $0.003H = 24$ mm (Schlosser et al. 1991).

**Table 7** The selected nail design parameters

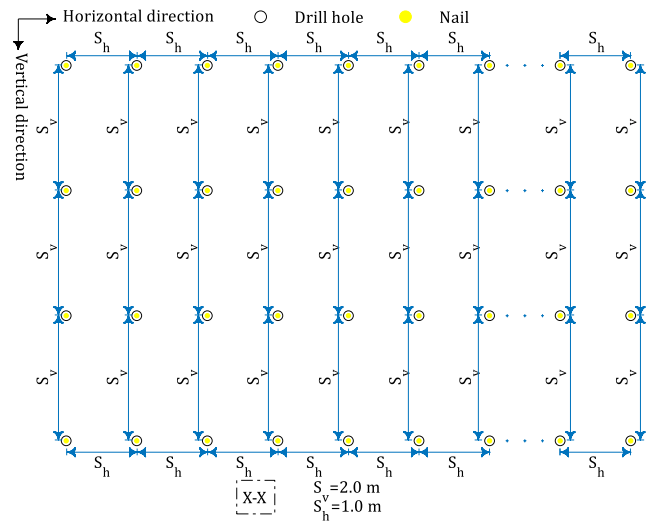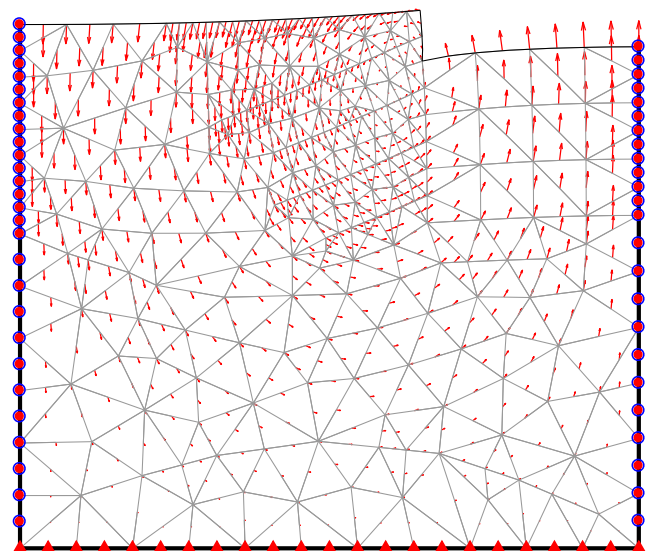| Parameters | Values |
| --- | --- |
| Nail elasticity modulus, $E_n$ (GPa) | 200.0 |
| Nail diameter, $d$ (mm) | 28.0 |
| Nail spacing, $S_h \times S_v$ (m × m) | 1.0 × 2.0 |
| Nail inclination with respect to the horizontal (Deg.) | 20.0 |



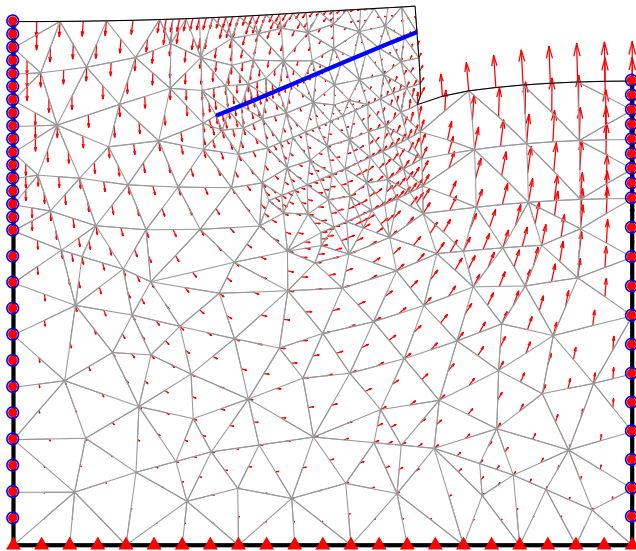**Fig. 12** Deformed mesh after 2.0-m excavation

**Fig. 13** Deformed mesh after 4.0-m excavation

Mobilized axial force distributions of the nails are presented in Fig. 18. It can be understood that the maximum tensile forces were mobilized in nail no. 3, where the adjacent wall had the maximum displacements. Based on the literature (Wei 2013), the development of soil nail forces is associated with the stages of construction. In other words, immediately after reaching subgrade and full excavation depth, the lowest row of the nails (i.e., nail no. 4) which was installed after the last stage of excavation (for improving the global stability), will have the least amount of tensile forces. However, nail forces tend to experience a moderate increase, up to approximately 15%, after the end of construction, over time, and for long-term conditions (Plumelle 1990). These post-construction increases in nail forces occur mainly due to soil creep and stress relaxation, which is not one of the research concerns herein.
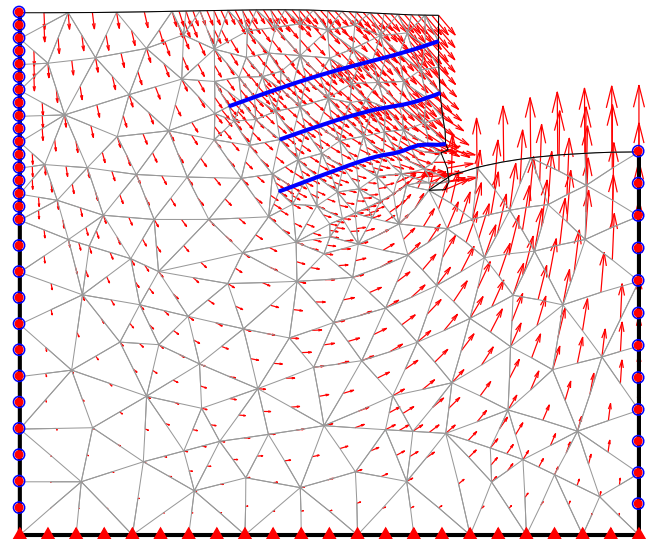


**Fig. 15** Deformed mesh after 8.0-m excavation

In another viewpoint, the distributions of tensile forces per nail length were shown in Fig. 19. The comparison between Figs. 19 and 21 indicates that the maximum tensile force location in nails occurred in the range of 0.40–0.65 of the nail length and close to the established critical slip surface in stability analyses.

## Stability analysis of the soil nail wall

In this research, more important types of stability of the soil nail wall, including global stability, soil nail tensile strength, and pullout, are considered.

**Global stability** In the current study, the nail axial stiffness was held constant, and using the methodology of strength reduction, the global safety factor of the soil nail wall was obtained.
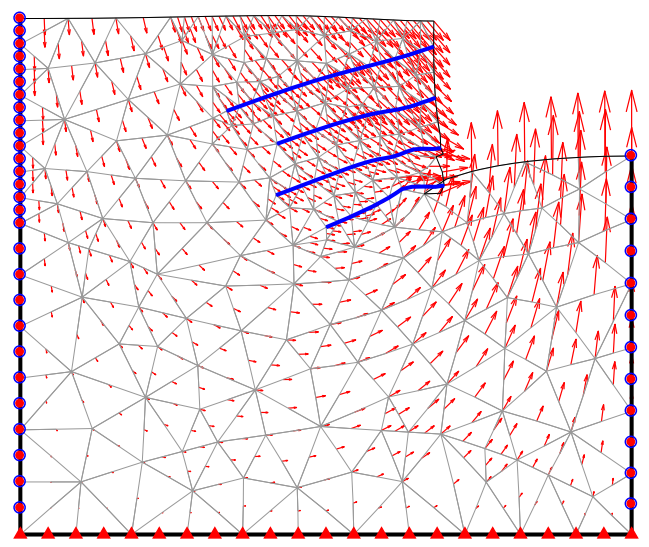


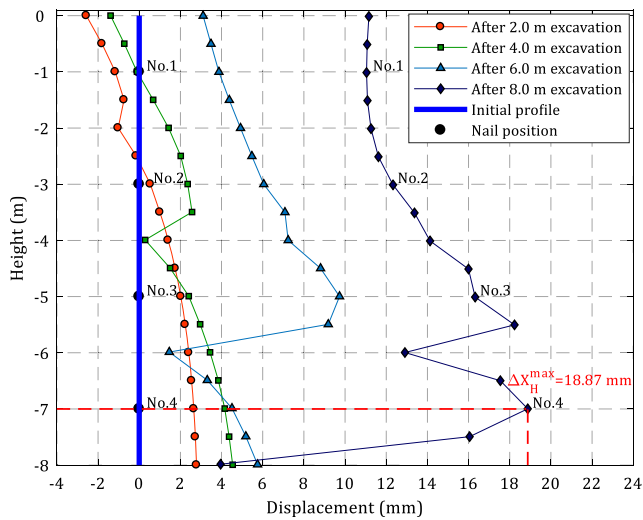**Fig. 14** Deformed mesh after 6.0-m excavation



**Fig. 16** Deformed mesh after 4th nail activation

Fig. 17 Wall profile after staged excavation



Fig. 19 Mobilized tensile forces in the nails

In this method, the first strength reduction factor that brings the soil nail wall to failure (convergence does not occur in a specified number of iterations) is taken as the SF. By this strategy, as given in Table 10, the safety factor of the model was determined to SF = 1.20, which has a logical interval from instability (SF = 1.0). Figure 20 indicates the displacement vectors and deformed mesh corresponding to the divergent solution at the final stage of excavation (depth of excavation = 8.0 m).

**Soil nail tensile strength stability** The soil nail tensile strength stability is obtained by dividing the nominal tensile resistance of nail ($R_t$) to maximum mobilized forces in the nails at the end of the construction process (Lazarte et al. 2015). In this example, $R_t = 255.54$ kN/m was calculated from the nail area ($A_n = 6.16$ cm$^2$) and yield strength of steel ($F_y = 415$ MPa). The maximum mobilized forces ($T_{max}$) in the nails were

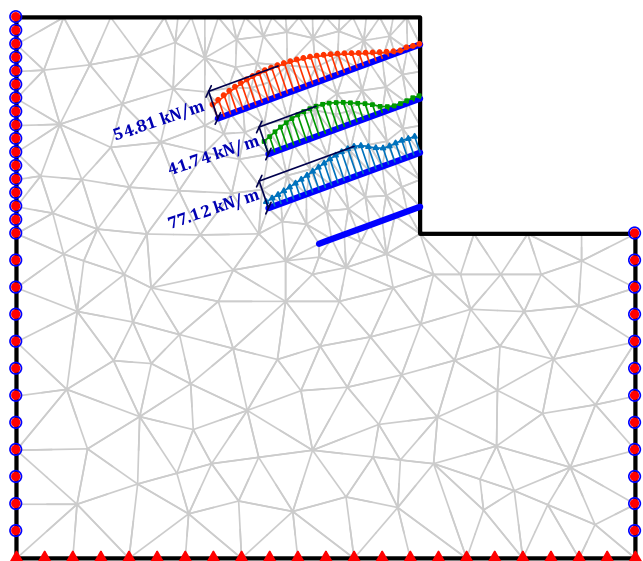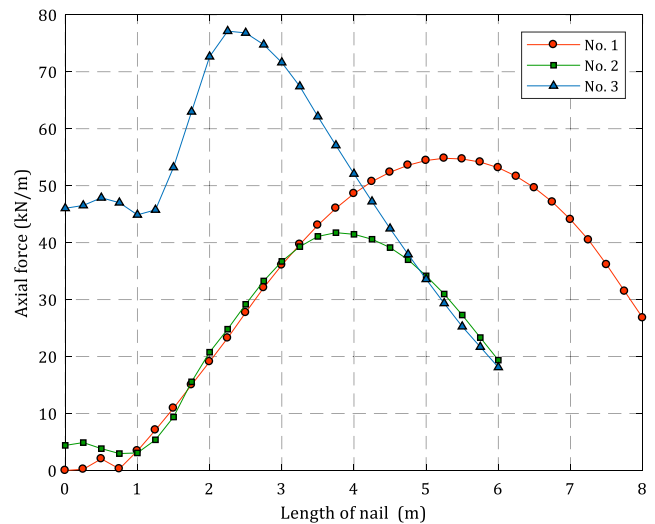shown in Figs. 18 and 19, which are 54.81, 41.74, and 77.12 kN/m for nail nos. 1 to 3 respectively. As a result, the factors of safety against nail tensile strength were determined and summarized in Table 10. It is worth mentioning that the SF against the tensile strength of the nail no. 4 is neglected and has not been mentioned in the following results.

**Soil nail pullout stability** It is obvious that conducting field pullout test is obligatory for high accuracy determination of the ultimate pullout resistance. However, due to a lack of excavation progression, a verified equation was used to determine the grout-ground interface pullout resistance. In this way, the allowable pullout resistance provided by the soil-grout bond strength in the passive zone ($P_{pullout}$) is expressed by following well-known equation (Schlosser and Guilloux 1981; Chan 2008; Watkins and Powell 1992; Cartier 1983):
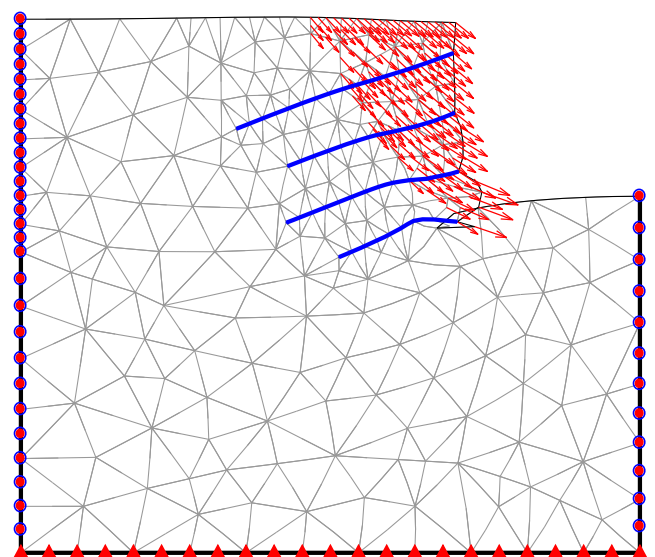


Fig. 18 Distribution of nail-mobilized tensile forces



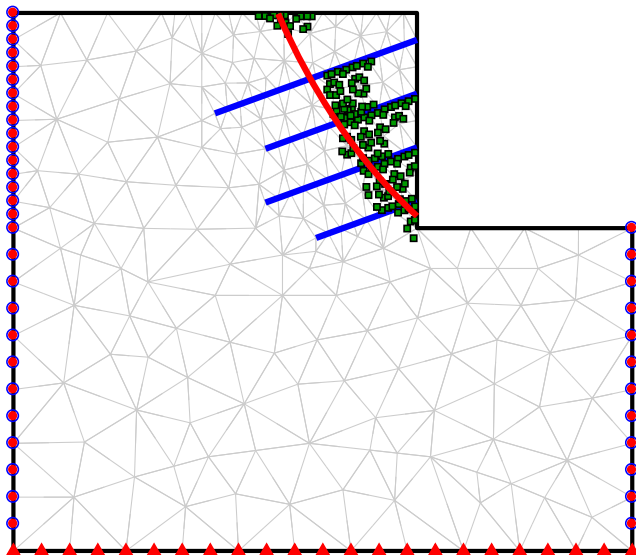Fig. 20 Displacement vectors and deformed mesh in unconverted solution

**Fig. 21** The obtained maximum accumulated deviatoric plastic strain using strength reduction

$$P_{\text{pullout}} = \left( \pi D_{\text{DH}} c' + 2 D_{\text{DH}} \sigma'_{v} \tan\left(\phi'\right) \right) L_p \quad (11)$$

where $c'$ is soil effective cohesion, $\sigma_{v}'$ is effective vertical stress at the mid-depth of the nail, $\phi'$ is soil effective friction angle, and $D_{\text{DH}}$ is drill hole diameter.

Since the passive length ($L_p$) of nails has been expressed as the length between the intersection of a soil nail with the slip surface and end of the nail; the slip surface needs to be determined. For this purpose, in this example, as shown in Fig. 21 at the final stage of the excavation after the shear strength reduction, the critical failure surface was determined using maximum accumulated deviatoric plastic strain. However, there are various methods to obtain the critical failure surface (Zhang and Wang 2016; Wei et al. 2009; Johari and Talebi
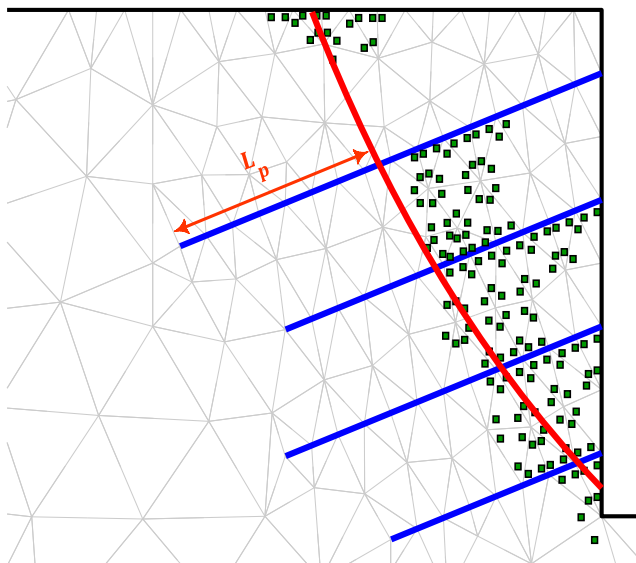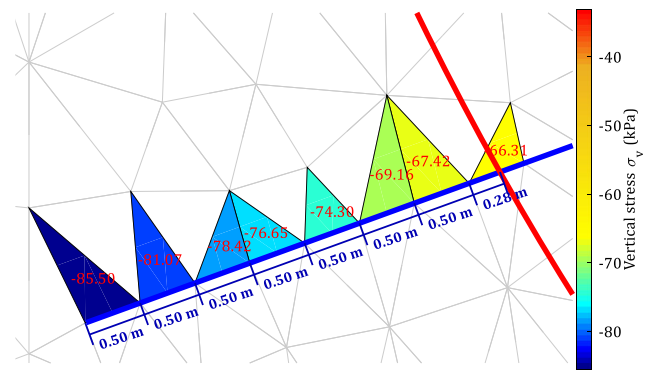


**Fig. 22** The effective length of the nails



**Fig. 23** Stress distribution along Lp of the nail no. 1 in an illustrative example

2019; Qi and Li 2018). Figure 22 shows the $L_p$ for the illustrated example.

To determine the $P_{\text{pullout}}$ of each nail, this value for each part of the nail, as shown in Fig. 23, was calculated, and the results were summarized. The detail of this procedure was given for nail no. 1 in Table 8. This strategy was repeated for all nails, and the results are summarized in Table 9. Finally, the safety factors against soil nail pullout were determined using $T_{\text{max}}$ and $P_{\text{pullout}}$ (SF = $P_{\text{pullout}}/T_{\text{max}}$). The results were given in Table 10. It should be noted that safety factor against soil nail pullout resistance of the nail no. 4 is neglected and has not been mentioned in the results.

**Lateral displacement safety factor** Based on past performance data of excavations through similar soil conditions, typical lateral displacements are expected to vary from 0.001H to 0.003H for walls built with a reasonable safety factor. This reasonable safety factor implies an acceptable performance for the soil nail wall. These values can be treated as upper bound (0.003H) and lower bound (0.001H) for the horizontal displacements. Therefore, particular attention was paid to designing the soil nail wall system to limit the movements and also to meet safety requirements. In this way, the allowable horizontal

**Table 8** $P_{\text{pullout}}$ calculation for the nail no. 1

| Nail | Parameters | | |
|---|---|---|---|
| | $\sigma_v'$ (kPa) | $(L_p)_i$ (m) | $(P_{\text{pullout}})_i$ (kN) |
| No. 1 | 66.31 | 0.28 | 4.29 |
| | 67.42 | 0.50 | 7.68 |
| | 69.16 | 0.50 | 7.77 |
| | 74.30 | 0.50 | 8.02 |
| | 76.65 | 0.50 | 8.14 |
| | 78.42 | 0.50 | 8.22 |
| | 81.07 | 0.50 | 8.35 |
| | 85.50 | 0.50 | 8.56 |
| $\Sigma$ | 598.82 | 3.78 | 61.05 |

**Table 9** Ultimate pullout resistance of the nails

| Ultimate pullout resistance (kN/m) | Values |
| --- | --- |
| Nail no. 1 | 61.05 |
| Nail no. 2 | 55.78 |
| Nail no. 3 | 96.01 |

displacement at the top of the wall has been chosen equal to 0.003H, which is a well-known deterministic margin value established from the upper bound of measurements from as-built structures. To obtain the safety factor of lateral displacement of the soil nail wall against loss of serviceability, allowable lateral displacement reported by the codes (0.003H) (Schlosser et al. 1991) is divided by maximum lateral displacement at the top of the wall. Such a procedure was also used for the tensile strength safety factor, where the deterministic nominal tensile resistance of nails was used for margin value. This safety factor is given in Table 10. The final view of the stabilized soil nail wall and excavation is shown in Fig. 24.

## Stochastic analysis of the soil nail wall

The deterministic coded program was extended to the probabilistic context to consider soil property fluctuation. In this way, the random fields were generated for normal distribution friction angle, cohesion, and unit weight in the MCS. The stochastic parameters with mean and standard deviation (Std.) which are excluded from Tables 3, 4, and 5 were presented in Table 11. A total of 1000 simulations were performed to implement the uncertainties of the soil properties. Based on the literature, an acceptable strategy for determining the probability density function (PDF) is to carry out reasonable MCS and fit a normal or lognormal function to the computed distribution of SF (Griffiths and Fenton 2008). The fitted distribution can then be used to determine the reliability index or probability of failure. The 273rd realization for cohesion, friction angle, and unit weight is shown in Figs. 25, 26, and 27, respectively. Furthermore, spatial variability of in

**Table 10** The obtained safety factors of stability modes

| Stability modes | Values |
| --- | --- |
| Global safety factor | 1.20 |
| Tensile strength SF of nail no. 1 | 4.66 |
| Tensile strength SF of nail no. 2 | 6.12 |
| Tensile strength SF of nail no. 3 | 3.31 |
| Pullout resistance SF of nail no. 1 | 1.11 |
| Pullout resistance SF of nail no. 2 | 1.33 |
| Pullout resistance SF of nail no. 3 | 1.24 |
| Lateral displacement SF | 2.15 |



**Fig. 24** Final view of soil nail wall and excavation

situ vertical stresses, which are affected by the unit weight fluctuation, is presented in Fig. 28.

The scale of fluctuation used in a random finite element analysis is more than double of element size (Huang and Griffiths 2015). The correlation length in $x$ and $y$ directions was assumed to be $l_x = 5.0$ m and $l_y = 3.0$ m, respectively. The cross-correlation coefficient between cohesion and friction angle was considered $\rho_{(c, \phi)} = -0.5$. A positive correlation between friction angle and unit weight is presented within the range of 0.1 to 0.7 (Luo et al. 2016; Wu 2013). In this study, this value was supposed as $\rho_{(\phi, \gamma)} = 0.7$.

To perform a stochastic analysis, the simulation was repeated to obtain the PDFs of the soil nail wall safety factors. In this way, to obtain the PDF of pullout resistance safety factor, using the advantages of RFEM, the locations of the maximum accumulated deviatoric plastic strain and, consequently, the slip surfaces were determined. Simultaneously, to demonstrate the reasonability of the conducted MSCs, the convergence study for various types of stability modes was performed and then shown in Figs. 29, 30, and 31. Figure 32 shows the variation of the slip surfaces due to soil parameter uncertainties. Based on the locations of the intersection of slip surface and nails, the intersection location distribution was determined as a normal distribution for each nail. As a result, the location of the intersections varied from 0.3L–0.9L for nail no. 1, 0.25L–0.95L for nail no. 2, and finally, 0.05L–0.7L for nail no. 3. This means the uncertainty of the soil parameters has the

**Table 11** Stochastic soil parameters

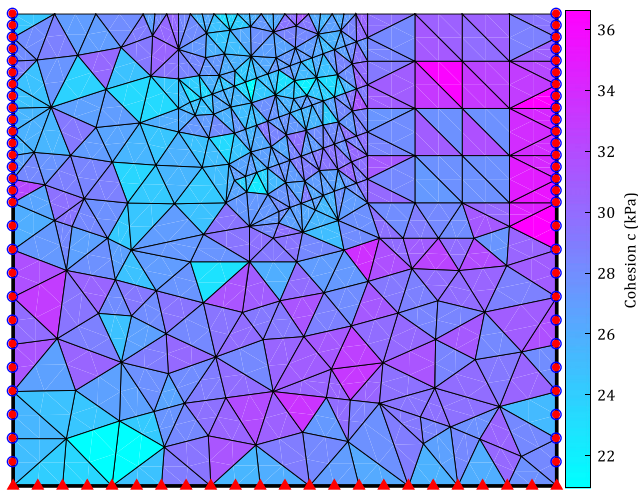| Soil parameters | Mean | Std. |
| --- | --- | --- |
| Cohesion, $c$ (kN/m$^2$) | 28.0 | 2.8 |
| Friction angle, $\phi$ (Deg.) | 26.0 | 2.6 |
| Unit weight, $\gamma$ (kN/m$^3$) | 18.0 | 0.9 |

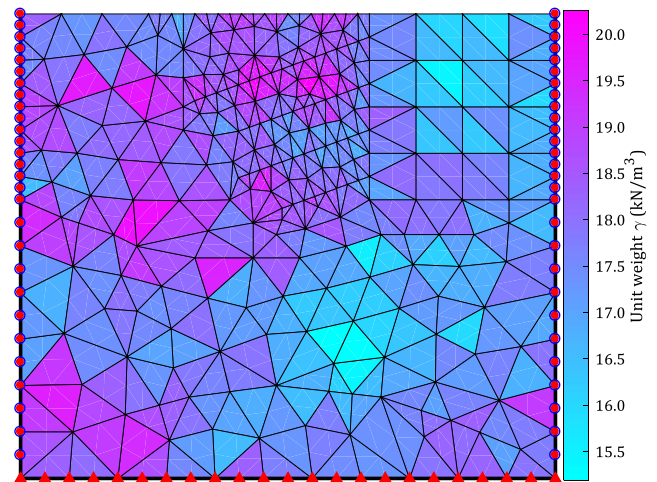**Fig. 25** A random field of 273rd realization for cohesion



**Fig. 27** A random field of 273rd realization for unit weight

most significant effect on $L_p$ and, consequently, the pullout resistance SF of the nail no. 2. The effect of these results can be seen in the Std. = 0.31 and coefficient of variation (COV) = 0.16 of the nail no. 2 in Table 12.

Since the variations of stochastic parameters were considered to be normal distributions, it seems sensible to suppose that the PDFs of the soil nail wall SF would also be normal. By using the mean, Std., and COV of the computed stochastic values of SF, which are collected in Table 12, both normal and lognormal distribution functions were fitted to each distribution. In all of these cases, the normal distribution showed more reasonable accuracy. As a result, the PDFs of the global safety factor, lateral displacement, tensile strength, and pullout resistance for all nails are shown in Figs. 33, 34, 35, and 36.

Based on Table 12, the COV of global safety factor and lateral displacement safety factors were calculated as 0.04 and 0.11, respectively. This means that the spatial variability of the soil parameters has a more significant effect on the variation of the lateral displacement safety factor.

According to Fig. 35, in tensile strength, the minimum safety factor correspond to nail no. 3, which had the maximum value of tensile forces. Furthermore, the maximum safety factor correspond to nail no. 2, which had the minimum value of tensile forces as obtained in the previous section. All three of the tensile strength safety factors have a logical interval from instability. In other words, the largest variation of the mentioned safety factors was attributed to nail no. 2, which means that the fluctuation of soil properties had a more significant effect on this safety factor.

From Fig. 36, it can be seen that the minimum mean of pullout resistance safety factor belongs to nail no. 1, which is due to a large value of tensile forces, wide variations of $L_p$, and the lowest value of effective vertical stress at the mid-depth of the nail in the resistance zone.

The stochastic lateral displacement profiles are shown in Fig. 37. Normal distribution was fitted to the stochastic lateral displacement at each depth of the nail position and top of the wall. The mean and Std. were found to be equal to 10.06 mm and 1.17 mm, respectively, at the top of the wall. The
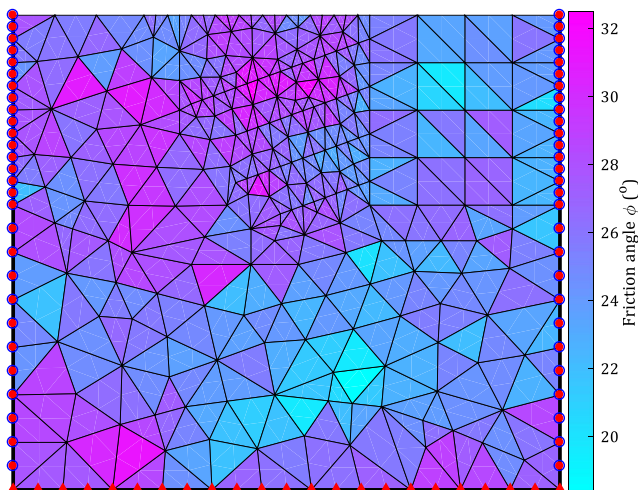


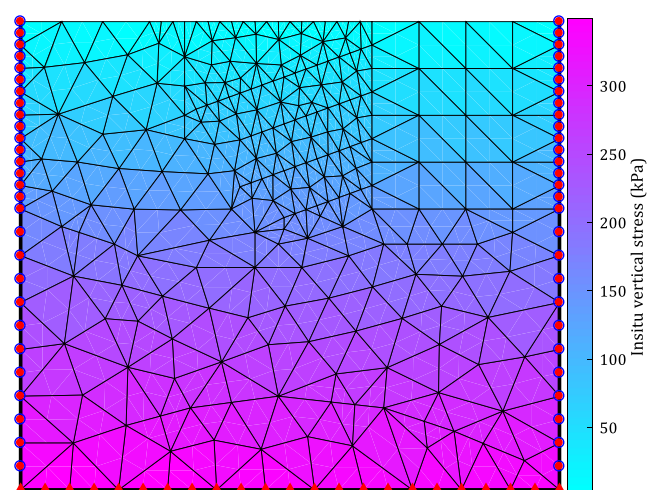**Fig. 26** A random field of 273rd realization for friction angle



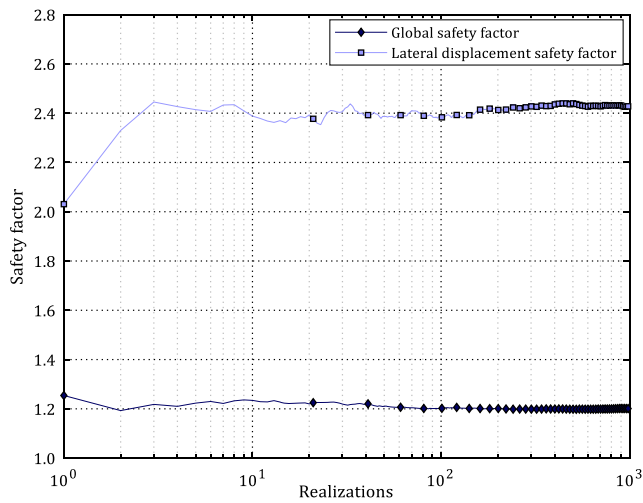**Fig. 28** A random field of 273rd realization for in situ vertical stresses

Fig. 29 Convergence study for global safety factor and lateral displacement safety factor



Fig. 31 Convergence study for pullout resistance safety factor for all nails

minimum and maximum lateral displacement at the top of the wall were 7.62 mm and 13.09 mm, respectively. According to this figure, the uncertainty of the soil parameters had the most significant effect on lateral displacements at the lowest level of the nails, no. 4 (the maximum Std. exists in this level).

## System reliability analysis of the soil nail wall

In the previous section, the PDFs of the system components of the soil nail wall were obtained. In this section, the system reliability analysis of the soil nail wall will be conducted. Since the soil nail wall has various components, for reliability analysis, the effects of these components should be considered. The soil nail wall system consists of four major components, which are global stability, tensile strength, pullout resistance, and lateral displacement. Two of those, tensile strength and pullout resistance, have three subsystem components (for each nail). Since instability in each component of
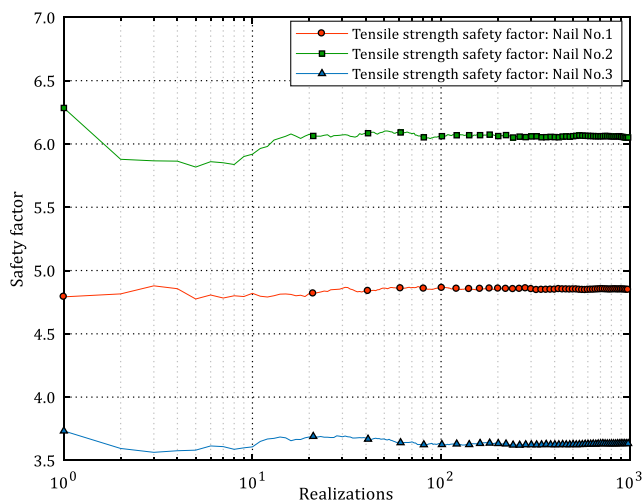
the soil nail wall causes instability of the wall, the assessed system is considered as a series system. For this purpose, the reliability index of each component must be obtained. The key advantage of the system modeling approach is that it provides a single index for quantifying the structure's overall reliability, instead of partial and unrelated components' reliabilities. This greatly facilitates the use of system reliability index as a criterion of design optimization and decision support. It is meant that, for example, in the event of failure of one or more nail, the wall does not necessarily collapse because the remaining nails assume additional responsibility in terms of loads, even if not as initially intended.

The reliability index ($\beta$), can be computed as Eq. (12), is an alternative measure of reliability, which is uniquely related to the probability of failure ($P_f$) as it is demonstrated in Eq. (13).

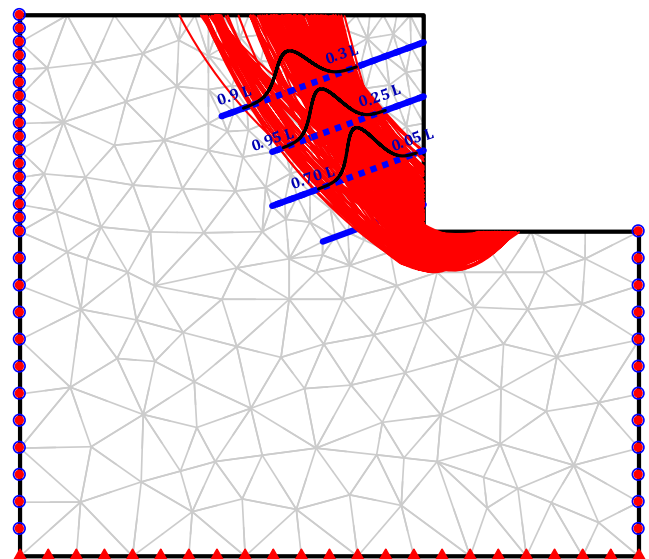$$\beta = \frac{M - \mu}{\sigma} \tag{12}$$



Fig. 30 Convergence study for tensile strength safety factor for all nails



Fig. 32 Stochastic slip surfaces obtained by strength reduction

**Table 12** The safety factor distribution statistical parameters

| Soil parameters | Mean | Std. | COV |
|---|---|---|---|
| Global safety factor | 1.20 | 0.05 | 0.04 |
| Tensile strength SF of nail no. 1 | 4.85 | 0.19 | 0.04 |
| Tensile strength SF of nail no. 2 | 6.06 | 0.31 | 0.05 |
| Tensile strength SF of nail no. 3 | 3.63 | 0.18 | 0.05 |
| Pullout resistance SF of nail no. 1 | 1.63 | 0.24 | 0.15 |
| Pullout resistance SF of nail no. 2 | 1.92 | 0.31 | 0.16 |
| Pullout resistance SF of nail no. 3 | 1.85 | 0.28 | 0.15 |
| Lateral displacement SF | 2.42 | 0.28 | 0.11 |

where $M$, $\mu$, and $\sigma$ are safety margin, mean, and standard deviation of the distribution, respectively.

$$p_f = 1 - \Phi(\beta) \quad (13)$$

where $\Phi(\beta)$ calculated as follows:

$$\Phi(\beta) = \int_{-\infty}^{\beta} \frac{1}{\sqrt{2\pi}} e^{-\frac{1}{2}x^2} dx \quad (14)$$

When SF has a normal distribution, the value of $\beta$ indicates the number of Std. between the critical value (SF = 1.0) and the most likely value for SF. The reliability indices of each component of the soil nail wall stability, which are calculated from their PDFs (Figs. 33, 34, 35, and 36), are presented in Table 13. Although the reliability indices can be influenced by the depth of excavation panels, the analysis was performed concerning the common procedure of excavation. Nonetheless, a sensitivity analysis can be done with regard to this effect.

To combine the components of the system (soil nail wall), the SCM was utilized. In this way, the correlation between the components should be estimated using their PDF data. These correlation factors show how many stability components are
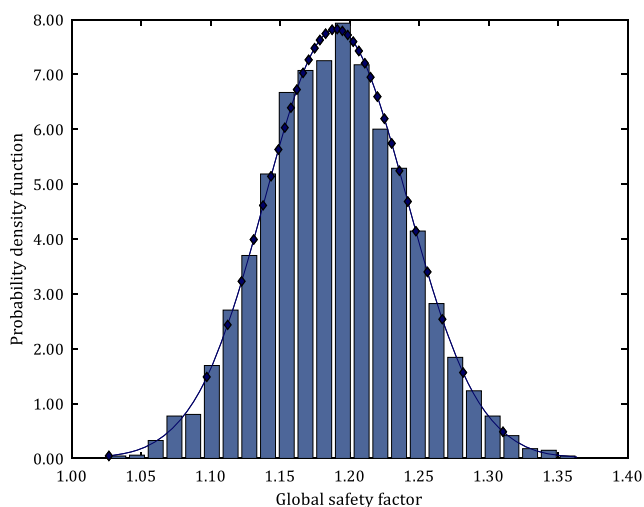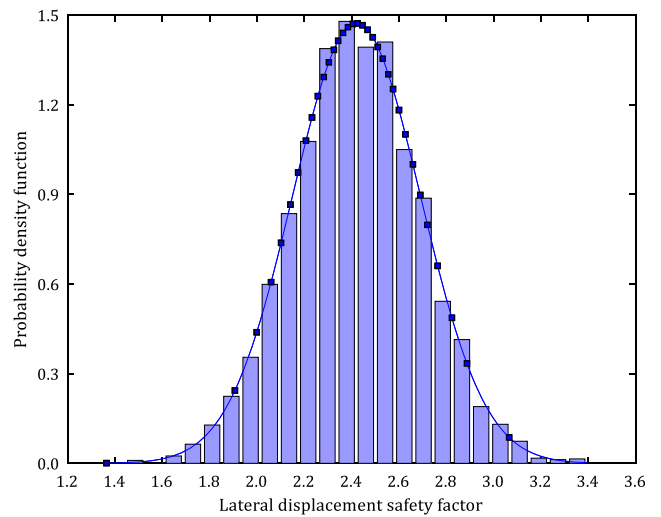


**Fig. 34** PDF of the lateral displacement safety factor

correlated. Two illustrative examples for determining the correlation between global safety factor and lateral displacement safety factor, and between tensile strength and pullout resistance safety factors for nail no. 3, were shown in Figs. 38 and 39, respectively. This procedure was repeated for all components, and the results were collected to the correlation matrix (Eq. (15)).

$$\rho = \begin{bmatrix} G & T_3 & T_2 & T_1 & P_3 & P_2 & P_1 & D & \\ 1 & 0.282 & 0.113 & 0.425 & 0.249 & 0.118 & 0.382 & 0.809 & G \\ & 1 & 0.243 & 0.420 & 0.578 & 0.190 & 0.239 & 0.576 & T_3 \\ & & 1 & 0.142 & 0.129 & 0.551 & 0.124 & 0.145 & T_2 \\ & & & 1 & 0.225 & 0.101 & 0.508 & 0.644 & T_1 \\ & & & & 1 & 0.338 & 0.337 & 0.336 & P_3 \\ & & & & & 1 & 0.275 & 0.121 & P_2 \\ & & & & & & 1 & 0.456 & P_1 \\ Sym. & & & & & & & 1 & D \end{bmatrix} \quad (15)$$

The significant value of correlations in the correlation matrix indicates the dependency between stability components. The correlation between global safety factor and lateral
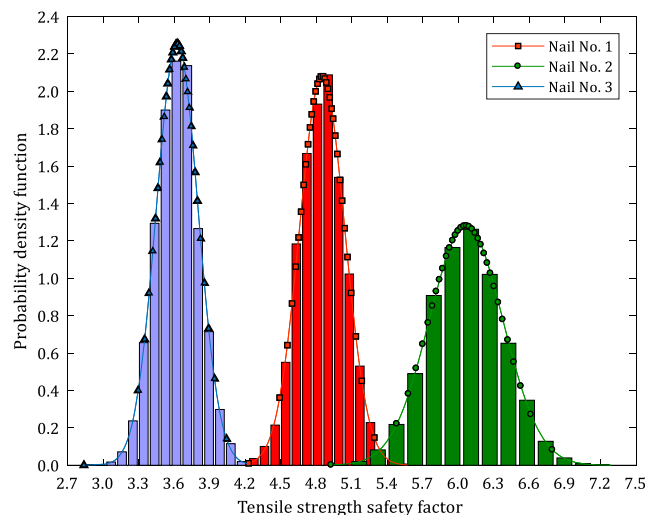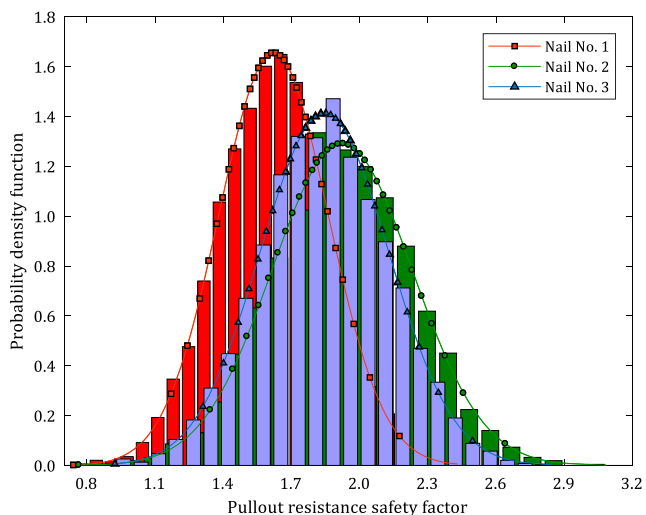


**Fig. 33** PDF of the global safety factor



**Fig. 35** PDSF of the tensile strength safety factor

**Fig. 36** PDSF of pullout resistance safety factor

**Table 13** Reliability indices of the soil nail wall components

| Components | Reliability index ($\beta$) | Probability of failure ($P_f$) |
|---|---|---|
| 1. Global stability | 3.782 | 7.5651E-05 |
| 2. Tensile strength | | |
| 2.1 Nail no. 1 | 20.126 | 0.0 |
| 2.2 Nail no. 2 | 16.152 | 0.0 |
| 2.3 Nail no. 3 | 14.590 | 0.0 |
| 3. Pullout resistance | | |
| 3.1 Nail no. 1 | 2.588 | 0.0048 |
| 3.2 Nail no. 2 | 2.988 | 0.0014 |
| 3.3 Nail no. 3 | 3.026 | 0.0012 |
| 4. Lateral displacement | 5.145 | 1.3390E-07 |

displacement safety factor is 0.809, which is the maximum correlation in the correlation matrix. This means that these two types of stability are more dependent on one another compared with any other two stabilities. It should be noted, since the tensile forces are common parameters between tensile strength and pullout resistance stability, a considerable correlation was observed between the aforementioned stability components.

Figure 40 shows the flowchart for the combination of the reliability index of the different components of the soil nail wall. According to this figure, the reliability index of the soil nail wall system is equal to $\beta_{system} = 2.496$. For the actual design of the soil nail wall, a reasonable value for the probability of failure ($P_f$) is 1%, which implies $\beta_{system} = 2.33$ (Luo et al. 2016). Base on this criterion, Fig. 40 indicates that the system reliability index ($\beta_{system} = 2.496$) is less than the
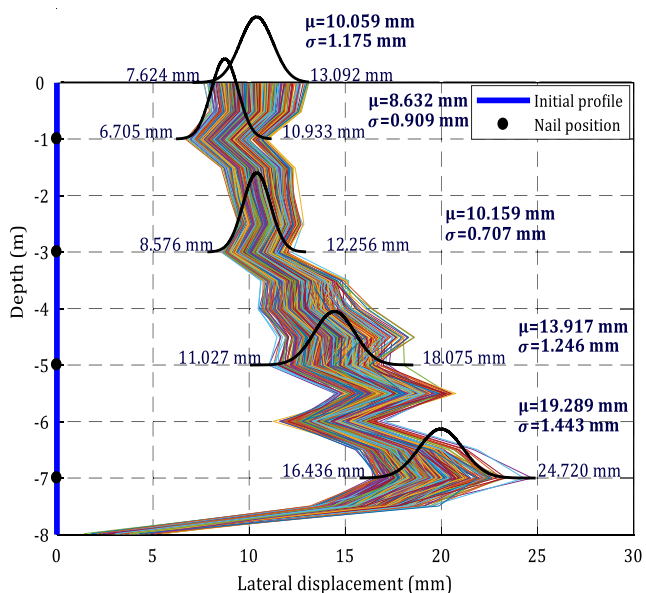
minimum reliability index of different components ($\beta_{min} = 2.588$) which both of the soil nail wall reliability indices are reasonable values for safe design.

From the US Army Corps of Engineers (Army 1995) viewpoint, as it is illustrated in Table 14, the performance level of the soil nail wall based on the minimum reliability index ($\beta_{min} = 2.588$) fell below the average category while the system reliability index ($\beta_{system} = 2.496$) would be classified as a poor design. Also, it can be observed that the failure probability of the system, which is $P_{f\_system} = 0.0063$ is higher than the highest probability of failure ($P_{f\_max} = 0.0048$) among the obtained values for different stability types.

## Conclusions

This paper presents the system reliability analysis of the soil nail wall via the random field theory and coupling with SCM. For this purpose, a real site of soil nail wall with an adjacent surcharge was considered. The staged excavation analysis for
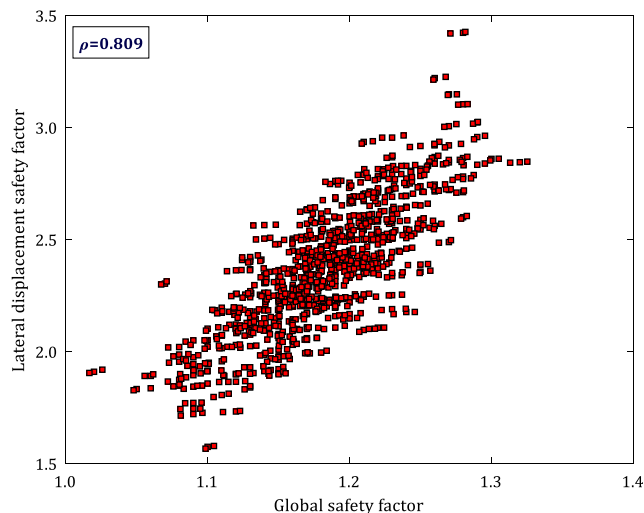


**Fig. 37** Stochastic lateral displacement after 8.0 m excavation



**Fig. 38** Determination of correlation between global safety factor and lateral displacement safety factor

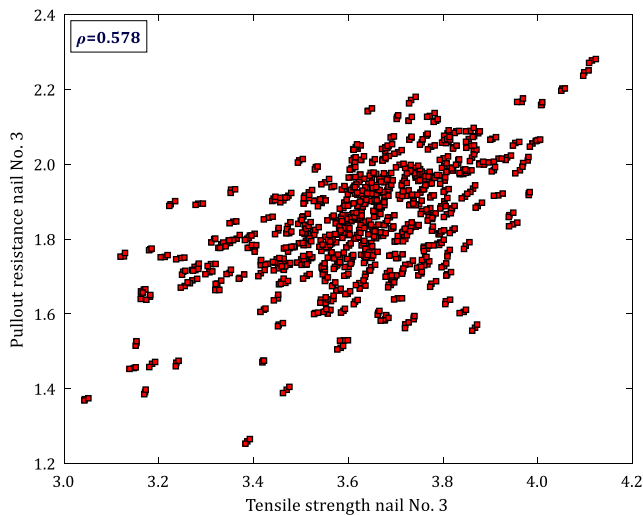Fig. 39 Determination of correlation between tensile strength and pullout resistance safety factors

**Table 14** Description of the reliability index and the probability of failure (Army 1995)

| Performance level | Reliability index ($\beta$) | Probability of failure ($P_f$) |
|---|---|---|
| High | 5.0 | 2.871E−7 |
| Good | 4.0 | 3.169E−5 |
| Above average | 3.0 | 0.00135 |
| Below average | 2.5 | 0.00621 |
| Poor | 2.0 | 0.02275 |
| Unsatisfactory | 1.5 | 0.06681 |
| Hazardous | 1.0 | 0.15866 |

calculation of the safety factors against global stability, tensile strength, pullout resistance, and lateral displacement serviceability was carried out through a two-dimensional finite element-based program coded in MATLAB. The analysis was performed deterministically and then was extended to the probabilistic context in order to take the spatial variability of soil properties into consideration. To achieve this aim, random fields were simulated by consideration of possible fluctuations of the soil properties. In another part of this paper, the system reliability analysis was conducted to determine the dependency of the soil nail wall stability modes. The most important observations can be summarized as follows:

- In the deterministic analysis, for the last stage of excavation, the maximum lateral displacement occurred at about 1.0 m from the bottom of the excavation. The maximum lateral displacement at the top of the wall was found to be equal to 11.16 mm, which is less than $0.003H = 24$ mm. Furthermore, the maximum tensile forces were mobilized, where the adjacent wall had the maximum displacements. The distribution of tensile forces per nail length showed that the location of maximum tensile forces in nails occurred in the range of 0.40–0.65 of the length of the nails and close to the established critical slip surface in the stability analyses.

- For the stochastic analysis, the random fields were generated for normal distributions of friction angle, cohesion, and unit weight in the MCS. Using the ability of RFEM, the locations of the maximum accumulated deviatoric plastic strain and, consequently, the slip surfaces were determined for all realizations. Based on the locations of
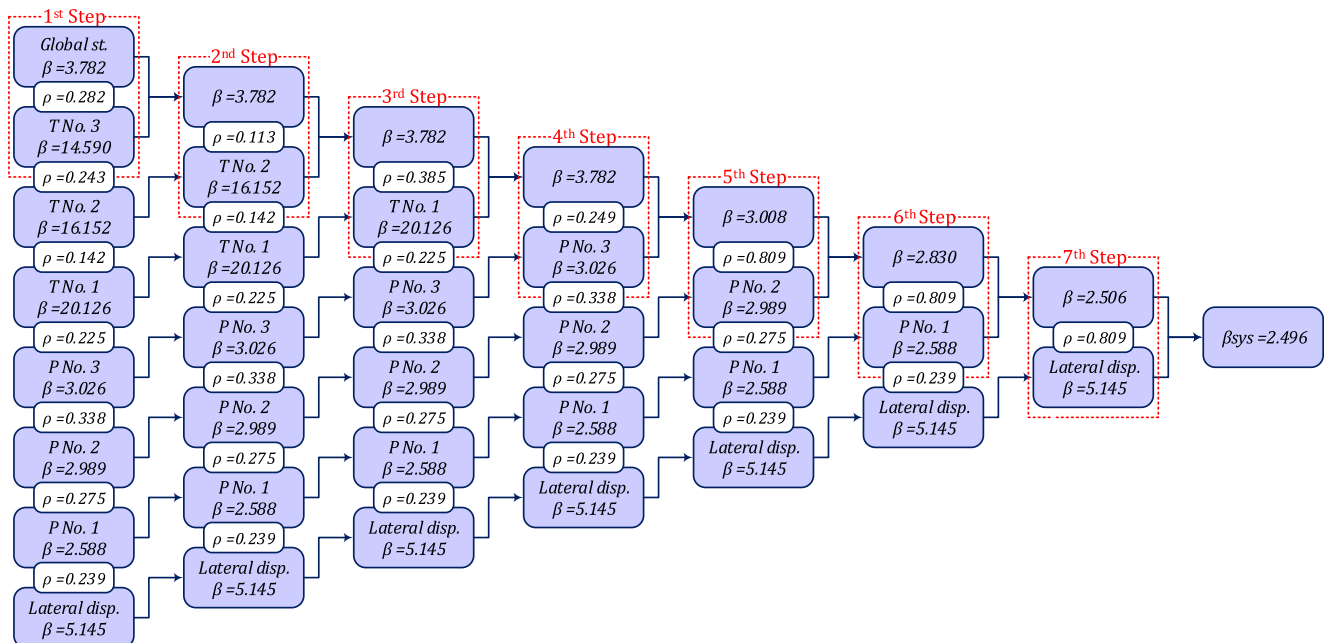


Fig. 40 The procedure of soil nail wall system reliability index determining

the intersection of the slip surface and nails, the intersection location distribution was determined as a normal distribution for each nail. As a result, the locations of the intersections varied from 0.3L–0.9L for nail no. 1, 0.25L–0.95L for nail no. 2, and finally, 0.05L–0.7L for nail no. 3. This means that the uncertainty of the soil parameters have the most significant effect on $L_p$ and, consequently, the pullout resistance SF of the second nail (no. 2).

- The COV of the global safety factor and the lateral displacement safety factor were calculated as 0.04 and 0.11, respectively. This means that the spatial variability of the soil parameters has a more significant effect on the variation of the lateral displacement safety factor.

- For the case of tensile strength, the minimum mean of the safety factor was corresponding to the nail, which had the maximum value of tensile forces (i.e., nail no. 3). On the other hand, the maximum mean value and the largest variety of the mentioned safety factor were attributed to the nail, which had a minimum value of tensile forces (i.e., nail no. 2). This means that the spatial variability of soil properties had a more significant effect on the tensile strength safety factor for this nail.

- Normal distribution was fitted to the stochastic lateral displacement at each depth of the nails and top of the wall. The mean and standard deviation were found to be equal to 10.06 mm and 1.17 mm, respectively, at the top of the wall. The minimum and maximum lateral displacements at the top of the wall were 7.62 mm and 13.09 mm, respectively. The uncertainty of the soil parameters had the most significant effect on lateral displacements at the lowest level of the nails.

- The soil nail wall has various components. For the sake of reliability analysis, the reliability index of each component of the system was obtained and combined via their correlations. For this purpose, the system was considered as a series. The correlation between the global safety factor and the lateral displacement safety factor was 0.809, which was the maximum correlation in the correlation matrix. This means that these two types of stability are more dependent on one another compared with any other two stabilities. Also, a considerable correlation was observed between the tensile strength and pullout resistance stability components.

- As expected from the serial system, the system reliability index ($\beta_{system}$ = 2.496) was less than the minimum reliability index of different components ($\beta_{min}$ = 2.588), and both were of reasonable values for safe design. The performance level of the soil nail wall based on the minimum

reliability index ($\beta_{min}$ = 2.588) fell below the average category, while the system reliability index ($\beta_{system}$ = 2.496) would be classified as a poor design. Also, it can be observed that the failure probability of the system, which is $P_{f\_system}$ = 0.0063 is higher than the highest probability of failure ($P_{f\_max}$ = 0.0048) among the obtained values for different stability types.

- In this study, the global safety factor, lateral displacement safety factor, tensile strength, and pullout resistance safety factor were investigated. System reliability analyses can be extended to the problem of facing stability in future researches. The actual system reliability is probably different than that computed by procedures noted in the paper due to pullout capacity estimation. Furthermore, still more effort shall be put on the problem of pullout resistance. All these efforts can be dedicated to developing a system reliability-based design framework for soil nail walls.

# Appendix

By using the information in Tables 1 and 7 which are presented in the paper, $E_n$ and $E_g$ values are as follows:

$$E_n = 200\text{GPa} \rightarrow 2 \times 10^8 kN/m^2 \tag{A.1}$$

$$E_g = 22\text{GPa} \rightarrow 2.2 \times 10^{7} kN/m^2 \tag{A.2}$$

By substituting the nail diameter in Eq. (A.3), nail cross-sectional area is obtained as follows:

$$A_n = \frac{\pi d_n^2}{4} \xrightarrow[d_n=0.028m]{d_n=28mm} = \frac{\pi (0.028)^2}{4} = 6.1575 \times 10^{-4} m^2 \tag{A.3}$$

By substituting the drilled hole diameter in Eq. (A.4), the hole cross-sectional area is obtained as follows:

$$A = \frac{\pi D^2_{DH}}{4} \xrightarrow{D_{DH}=0.10m} A = \frac{\pi (0.10)^2}{4}$$
$$= 78.5398 \times 10^{-4} m^2 \tag{A.4}$$

By substituting the drilled hole and nail cross-sectional area in Eq. (A.5), grout cross-sectional area is obtained as follows. The grout cross-sectional area is presented in Eq. (A.6)

$$A_g = A - A_n \xrightarrow[A=78.5398\times10^{-4}m^2]{A_n=6.1575\times10^{-4}m^2} A_g$$
$$= (78.5398 - 6.1575) \times 10^{-4} m^2 \tag{A.5}$$

$$A_g = 72.3823 \times 10^{-4} m^2 \tag{A.6}$$

By substituting the $E_n$ (Eq. (A.1)), $A_n$ (Eq. (A.3)), $E_g$ (Eq. (A.2)), $A_g$ (Eq. (A.6)), and hole cross-sectional area (A (Eq. (A.4))) in Eq. (A.7), the axial rigidity is determined as Eq. (A.8).

$$\mathrm{EA} = \frac{\left(E_n A_n + E_g A_g\right)\left(\pi D^2_{\mathrm{DH}}\right)}{4AS_h} = \frac{\left[\left(2\times 10^8\right)\left(6.1575\times 10^{-4}\right) + \left(2.2\times 10^7\right)\left(72.3823\times 10^{-4}\right)\right]\left(\pi 0.10^2\right)}{4\times 78.5398\times 10^{-4}\times 1} \tag{A.7}$$

$$\mathrm{EA} = 2.8239\times 10^{5} \, kN/m \tag{A.8}$$

# References

ACI Committee and International Organization for Standardization (2008). Building code requirements for structural concrete (ACI 318-08) and commentary. American Concrete Institute

Allahverdizadeh, P., D. Griffiths, and G. Fenton (2015), The random finite element method (RFEM) in probabilistic slope stability analysis with consideration of spatial variability of soil properties, in IFCEE 2015. p. 1946–55

Army US (1995) Introduction to probability and reliability methods for use in geotechnical engineering. Eng Tech Letter 1110-2:547

Babu GS, Singh VP (2009a) Reliability analysis of soil nail walls. Georisk 3(1):44–54

Babu G, Singh VP (2009b) Simulation of soil nail structures using PLAXIS 2D. Plaxis Bulletin 25:16–21

Babu GS, Rao R, Dasaka S (2007) Stabilisation of vertical cut supporting a retaining wall using soil nailing: a case study. Proc Inst Civil Eng Ground Improv 11(3):157–162

Bathurst RJ, Lin P, Allen T (2018) Reliability-based design of internal limit states for mechanically stabilized earth walls using geosynthetic reinforcement. Can Geotech J 56(6):774–788

Bryne, R (1998) Manual for design and construction monitoring of soil nail wall. Federal Highway Administration

Byrne R, Cotton D, Porterfield J, Wolschlag C, Ueblacker G (1996) Manual for design and construction monitoring of soil nail walls. Federal Highway Administration, United States (No. FHWA-SA-96-069)

Cartier G (1983) Experiments and observations on soil nailing structures. in Proc. of 8th European Conf. on SMFE

Chan RKS (2008) Geoguide 7, guide to soil nail design and construction. Geotechnical Engineering Office, Hong Kong

Chang G (2008) Optimization design of composite soil-nailing in loess excavation. In: Geotechnical Aspects of Underground Construction in Soft Ground: Proceedings of the 6th International Symposium (IS-Shanghai 2008). CRC Press, p 133

Cho SE (2009) Probabilistic assessment of slope stability that considers the spatial variability of soil properties. J Geotech Geoenviron 136(7):975–984

Cho SE (2013) First-order reliability analysis of slope considering multiple failure modes. Eng Geol 154:98–105

Da Costa A, Sagaseta C (2010) Analysis of shallow instabilities in soil slopes reinforced with nailed steel wire meshes. Eng Geol 113(1–4):53–61

Davies MCR, Jones AM, Kimura T, Kusakabe O, Takemura J (1998) Stability of a steep excavation retained by soil nails. Proceedings of Centrifuge '98, Vol. 1, A. A. Balkema, Rotterdam, 773–8

El-Ramly H, Morgenstern N, Cruden D (2002) Probabilistic slope stability analysis for practice. Can Geotech J 39(3):665–683

Fan C-C, Luo J-H (2008) Numerical study on the optimum layout of soil–nailed slopes. Comput Geotech 35(4):585–599

Fenton GA (1999) Estimation for stochastic soil models. J Geotech Geoenviron 125(6):470–485

Gassler G (1996) Design of reinforced excavations and natural slopes using new European code. In: Proceedings of International Symposium on Earth Reinforcement. Balkema AA, Rotterdam, pp 943–962

George P (1991) Automatic mesh generation: application to finite element method. Wiley Publishers

Griffiths DV, Fenton GA (2008) Risk assessment in geotechnical engineering. Wiley, Hoboken

Huang J, Griffiths D (2015) Determining an appropriate finite element size for modelling the strength of undrained random soils. Comput Geotech 69:506–513

Javankhoshdel S, Luo N, Bathurst RJ (2017) Probabilistic analysis of simple slopes with cohesive soil strength using RLEM and RFEM. Georisk: Assessment and Management of Risk for Engineered Systems and Geohazards 11(3):231–246

Jewell R, Pedley M (1992) Analysis for soil reinforcement with bending stiffness. J Geotech Eng 118(10):1505–1528

Johari A, Gholampour A (2018) A practical approach for reliability analysis of unsaturated slope by conditional random finite element method. Comput Geotech 102:79–91

Johari A, Heydari A (2018) Reliability analysis of seepage using an applicable procedure based on stochastic scaled boundary finite element method. Eng Anal Bound Elem 94:44–59

Johari A, Javadi A (2012) Reliability assessment of infinite slope stability using the jointly distributed random variables method. Scientia Iranica 19(3):423–429

Johari, A. and S. Mousavi, An analytical probabilistic analysis of slopes based on limit equilibrium methods. Bull Eng Geol Environ, 2018: p. 1–15

Johari A, Talebi A (2019) Stochastic analysis of rainfall-induced slope instability and steady-state seepage flow using random finite-element method. Int J Geomech 19(8):04019085

Kang W-H, Song J (2010) Evaluation of multivariate normal integrals for general systems by sequential compounding. Struct Saf 32(1):35–41

Kitch, W. (1994), Deterministic and probabilistic analyses of reinforced soil slopes. PhD diss., University of Texas, Austin

Lazarte, CA 2011 Proposed specifications for LRFD soil-nailing design and construction. Vol. 701, Transportation Research Board

Lazarte, C., H. Robinson, J. Gómez, A. Baxter, A. Cadden, and R. Berg (2015) Geotechnical engineering circular No. 7 soil nail walls—Reference manual. Rep. No. FHWA-NHI-14-007, Federal Highway Administration, Washington, DC

Li J, Tham L, Junaideen S, Yue Z, Lee C (2008) Loose fill slope stabilization with soil nails: full-scale test. J Geotech Geoenviron 134(3):277–288

Li D, Zhou C, Lu W, Jiang Q (2009) A system reliability approach for evaluating stability of rock wedges with correlated failure modes. Comput Geotech 36(8):1298–1307

Li D-Q, Jiang S-H, Cao Z-J, Zhou W, Zhou C-B, Zhang L-M (2015) A multiple response-surface method for slope reliability analysis considering spatial variability of soil properties. Eng Geol 187:60–72

Li X-Y, Zhang L-M, Gao L, Zhu H (2017) Simplified slope reliability analysis considering spatial soil variability. Eng Geol 216:90–97

Lin P, Bathurst RJ (2018) Reliability-based internal limit state analysis and design of soil nails using different load and resistance models. J Geotech Geoenviron 144(5):04018022

Lin P, Liu J (2017) Analysis of resistance factors for LFRD of soil nail walls against external stability failures. Acta Geotech 12(1):157–169

Lin P, Liu J, Yuan X-X (2016) Reliability analysis of soil nail walls against external failures in layered ground. J Geotech Geoenviron 143(1):04016077

Liu L-L, Deng Z-P, Zhang S-h, Cheng Y-M (2018) Simplified framework for system reliability analysis of slopes in spatially variable soils. Eng Geol 239:330–343

Low B, Tang WH (1997) Reliability analysis of reinforced embankments on soft ground. Can Geotech J 34(5):672–685

Luo N, Bathurst RJ, Javankhoshdel S (2016) Probabilistic stability analysis of simple reinforced slopes by finite element method. Comput Geotech 77:45–55

Pedley, MJ 1990 The performance of soil reinforcement in bending and shear. PhD diss., University of Oxford

Plumelle C (1990) French national research project on soil nailing: Clouterre. in Proc. of a Conf. on Design and Performance of Earth Retaining Structures

Puła W, Chwała M (2015) On spatial averaging along random slip lines in the reliability computations of shallow strip foundations. Comput Geotech 68:128–136

Qi X-H, Li D-Q (2018) Effect of spatial variability of shear strength parameters on critical slip surfaces of slopes. Eng Geol 239:41–49

Schlosser F, Guilloux A (1981) Le frottement dans le renforcement des sols. Rev Fr Géotech 16:65–77

Schlosser, F., Gigan, J.P. and Plumelle, C. (1991) Recommendations Clouterre/Soil Nailing Recommendations. French National Research Project Report, No. FHWA-SA-93_026

Shen C, Bang S, Herrman L (1981) Ground movement analysis of earth support system. J Geotech Geoenviron Eng (107) (ASCE 16732)

Shiu, Y. and G. Chang (2006) Effects of inclination, length pattern and bending stiffness of soil nails on behaviour of nailed structures. Geotechnical Engineering Office, Civil Engineering and Development Department

Sivakumar Babu G, Singh VP (2011) Reliability-based load and resistance factors for soil-nail walls. Can Geotech J 48(6):915–930

Smith I, Ho D (1992) Influence of construction technique on the performance of a braced excavation in marine clay. Int J Numer Anal Methods Geomech 16(12):845–867

Smith I, Su N (1997) Three-dimensional FE analysis of a nailed soil wall curved in plan. Int J Numer Anal Methods Geomech 21(9):583–597

Smith IM, Griffiths DV, Margetts L (2013) Programming the finite element method. Wiley

Stoker, M, Korber G, Gassler G, and Gudehus G (1979) Soil nailing. International Conference on Soil Reinforcement. Paris, France, Vol. 2, p. 469–474

Tan S, Ooi P, Park T, Cheang W (2008) Rapid pullout test of soil nail. J Geotech Geoenviron 134(9):1327–1338

Tei K, TAYLOR NR, Milligan GW (1998) Centrifuge model tests of nailed soil slopes. Soils Found 38(2):165–177

UK Department of Transport Design methods for the reinforcement of highway slopes by reinforced soil and soil nailing techniques (1994). Design Manual for Roads and Bridges 4, Part-4

Vanmarcke E (1980) Probabilistic stability analysis of earth slopes. Eng Geol 16(1–2):29–50

Vanmarcke E (2010) Random fields: analysis and synthesis. World Scientific

Watkins A, Powell G (1992) Soil nailing to existing slopes as landslip preventive works. Hong Kong Eng 20(3):20–27

Wei, Y. (2013) Development of equivalent surcharge loads for the design of soil nailed segment of MSE/soil nail hybrid retaining walls based on results from full-scale wall instrumentation and finite element analysis. PhD diss., Texas Tech University

Wei W, Cheng Y, Li L (2009) Three-dimensional slope failure analysis by the strength reduction and limit equilibrium methods. Comput Geotech 36(1–2):70–80

Wu XZ (2013) Trivariate analysis of soil ranking-correlated characteristics and its application to probabilistic stability assessments in geotechnical engineering problems. Soils Found 53(4):540–556

Zeng P, Jimenez R, Jurado-Piña R (2015) System reliability analysis of layered soil slopes using fully specified slip surfaces and genetic algorithms. Eng Geol 193:106–117

Zevgolis IE, Daffas ZA (2018) System reliability assessment of soil nail walls. Comput Geotech 98:232–242

Zhang G, Wang L (2016) Integrated analysis of a coupled mechanism for the failure processes of pile-reinforced slopes. Acta Geotech 11(4):941–952

Zhang M, Song E, Chen Z (1999) Ground movement analysis of soil nailing construction by three-dimensional (3-D) finite element modeling (FEM). Comput Geotech 25(4):191–204

Zhang J, Zhang L, Tang WH (2011) New methods for system reliability analysis of soil slopes. Can Geotech J 48(7):1138–1148

Zhao L-H, Zuo S, Li L, Lin Y-H, Zhang Y-B (2016) System reliability analysis of plane slide rock slope using Barton-Bandis failure criterion. Int J Rock Mech Min Sci 88:1–11